GEOLOGICAL SURVEY OF CANADA
OPEN FILE 6736

Configuration of Mike21 for the Simulation of Nearshore Storm Waves, Currents and Sediment Transport: Brackley Bight, Prince Edward Island

G.K. Manson

2012

Natural Resources Canada | Ressources naturelles Canada

Canada

GEOLOGICAL SURVEY OF CANADA
OPEN FILE 6736

Configuration of Mike21 for the Simulation of Nearshore Storm Waves, Currents and Sediment Transport: Brackley Bight, Prince Edward Island

G.K. Manson[1,2]

[1] Geological Survey of Canada - Atlantic, Bedford Institute of Oceanography, Dartmouth, NS
[2] Department of Geography, University of Guelph, Guelph, ON

2012

doi:10.4095/291980

This publication is available for free download through GEOSCAN (http://geoscan.ess.nrcan.gc.ca/).

Recommended citation
Manson, G.K., 2012. Configuration of Mike21 for the simulation of nearshore storm waves, currents, and sediment transport: Brackley Bight, Prince Edward Island, Geological Survey of Canada, Open File 6736, 33 p. doi:10.4095/291980

Publications in this series have not been edited; they are released as submitted by the author.
Cover photo: Brackley Beach from GSC site 1006 (GKM, GSC, October 19, 2007)

Table of Contents

Abstract **1**

Résumé **1**

Introduction **2**

Previous Fieldwork **3**
1999 Field Experiment (Hudson 99049) **3**
Marine Surveys **3**
Terrestrial Surveys **5**

Configuration of Mike21 ..... **6**
Model Domain **6**
DEM *6*
Mesh and Domain Boundaries *7*
Spectral Wave and Hydrodynamic Modules **9**
Solution Techniques *9*
Boundary Conditions *9*
Hindcast Winds *10*
Wave Breaking *10*
Wind Forcing *11*
Bottom Friction and Bed Resistance *11*
Wind Friction *12*
Sand Transport Module **14**
Layer Thickness *14*
STPQ3D *14*
Morphology Module *15*
Revisiting the Sediment Class Definitions *18*

Evaluation of the Adopted Configuration (Run28) **21**

Conclusions **27**

Acknowledgements **28**

References **29**

Configuration of Mike21 for the Simulation of Nearshore Storm Waves, Currents and Sediment Transport: Brackley Bight, Prince Edward Island

G.K. Manson[1,2]
[1] Geological Survey of Canada - Atlantic, Bedford Institute of Oceanography, Dartmouth, NS
[2] Department of Geography, University of Guelph, Guelph, ON

Abstract

The North Shore of Prince Edward Island (PEI) is a sandy, multi-barred coast with limited fetch in most directions but open to the Gulf of St. Lawrence for several hundred kilometres to the north. In the fall and winter, storms tracking northwards across PEI and into the Gulf can bring sustained storm waves which generate currents capable of transporting sand in both the along- and across-shore directions. Mike21 is a commercially available combined wave, hydrodynamic and sand transport model that may be utilised to improve understanding of contemporary sand transport and possible implications of changing climate in the Brackley Bight area of the North Shore. This manuscript describes the development of a Mike21 model domain and optimal configurations of the Mike21 Spectral Wave, Hydrodynamic and Sand Transport modules appropriate to the study area. The sensitivities of several parameters in each module are tested. The Spectral Wave and Hydrodynamic modules are sensitive to estimates of bed roughness with optimal values considerably lower than published semi-empirical estimates. The Sand Transport module is sensitive to the input sediment transport tables and estimates of the maximum amount of vertical bed level change per day. Simulation of a 4-day moderate northeasterly storm is conducted and the results are compared to currents, waves, and tides measured by S4 current meters and the instrumented seabed lander RALPH during a sediment transport experiment in 1999. The model successfully simulates storm waves and currents and provides reasonable estimates of the amount and patterns of sediment transport.

Résumé

La côte nord de l'Île-du-Prince-Édouard (Î.-P.-É.) est sableuse et parsemée de multiples cordons littoraux. Le fetch y est limité dans la plupart des directions sauf vers le nord, dans le golfe du Saint-Laurent, où il s'étend sans obstacle sur plusieurs centaines de kilomètres. En automne et en hiver, les tempêtes en direction nord qui traversent l'île vers le golfe peuvent créer dans la région des ondes de tempête soutenues qui génèrent des courants capables de transporter le sable le long de la côte et perpendiculairement à cette dernière. Mike21 est un modèle combiné de vagues, de phénomènes hydrodynamiques et de transport du sable disponible dans le commerce qui peut servir à améliorer notre connaissance du transport du sable et des répercussions possibles de l'évolution du climat dans la zone de la baie Brackley, sur la côte nord de l'Île-du-Prince-Édouard. Le présent document décrit la mise au point d'un domaine du modèle Mike21 et les configurations optimales des modules de houle spectrale, d'hydrodynamique et de transport du sable adaptés à la zone d'étude. On évalue la sensibilité de plusieurs paramètres dans chaque module. Les modules de houle spectrale et d'hydrodynamique sont sensibles aux estimations de la rugosité du fond marin et donnent des valeurs optimales beaucoup plus faibles que les estimations semi-empiriques publiées. Le module de transport du sable est sensible aux données d'entrée des tableaux de transport des sédiments et aux estimations des variations verticales quotidiennes maximales du niveau du fond marin. Les résultats de la simulation d'une tempête du nord-est d'intensité modérée d'une durée de quatre jours sont comparés aux valeurs des courants, des vagues et des marées mesurées à l'aide d'un courantomètre de type S4 et du module benthique instrumenté RALPH dans le cadre d'une expérience sur le transport des sédiments réalisée en 1999. Le modèle a simulé avec succès les ondes de tempête et les courants, et a fourni des estimations raisonnables de l'ampleur et des caractéristiques du transport des sédiments.

Introduction

The informally named Brackley Bight lies on the North Shore of Prince Edward Island in the southern Gulf of St. Lawrence (Fig. 1). Due to a combination of postglacial subsidence and sea-level rise from eustatic and steric effects, relative sea level (RSL) has risen from a lowstand of -42 m at approximately 9.5 ka. Based on the Charlottetown tide gauge record between 1911 and 1998, the rate of RSL rise has been 3.2 mm/a (Parkes et al., 2002). This postglacial transgression has resulted in the present day shoreline which consists of submergent embayments, mixed sandstone and till cliffs, scarped dunes, and sandy deposits in beaches, spits, dunes and ebb- and flood-tidal deltas. Despite an apparent abundance of sand in these depositional sinks, between approximately 7 and 35 m water depth, sand is relatively scarce and found in thin disconnected sheets (Forbes and Manson, 2002). Alongshore drift is considered constrained by subtle headlands to discrete, multi-barred cells (Forbes et al., 2004). Brackley Bight is one of these cells lying between Orby Head and Cape Stanhope (Fig. 2). Due to the above conditions and an abundance of archived data, Brackley Bight has been selected as a suitable area to test a sediment dynamics modelling approach towards understanding and quantifying climate change impacts on nearshore sediment transport with the potential to give insight into future shoreline morphology and sediment transport processes.

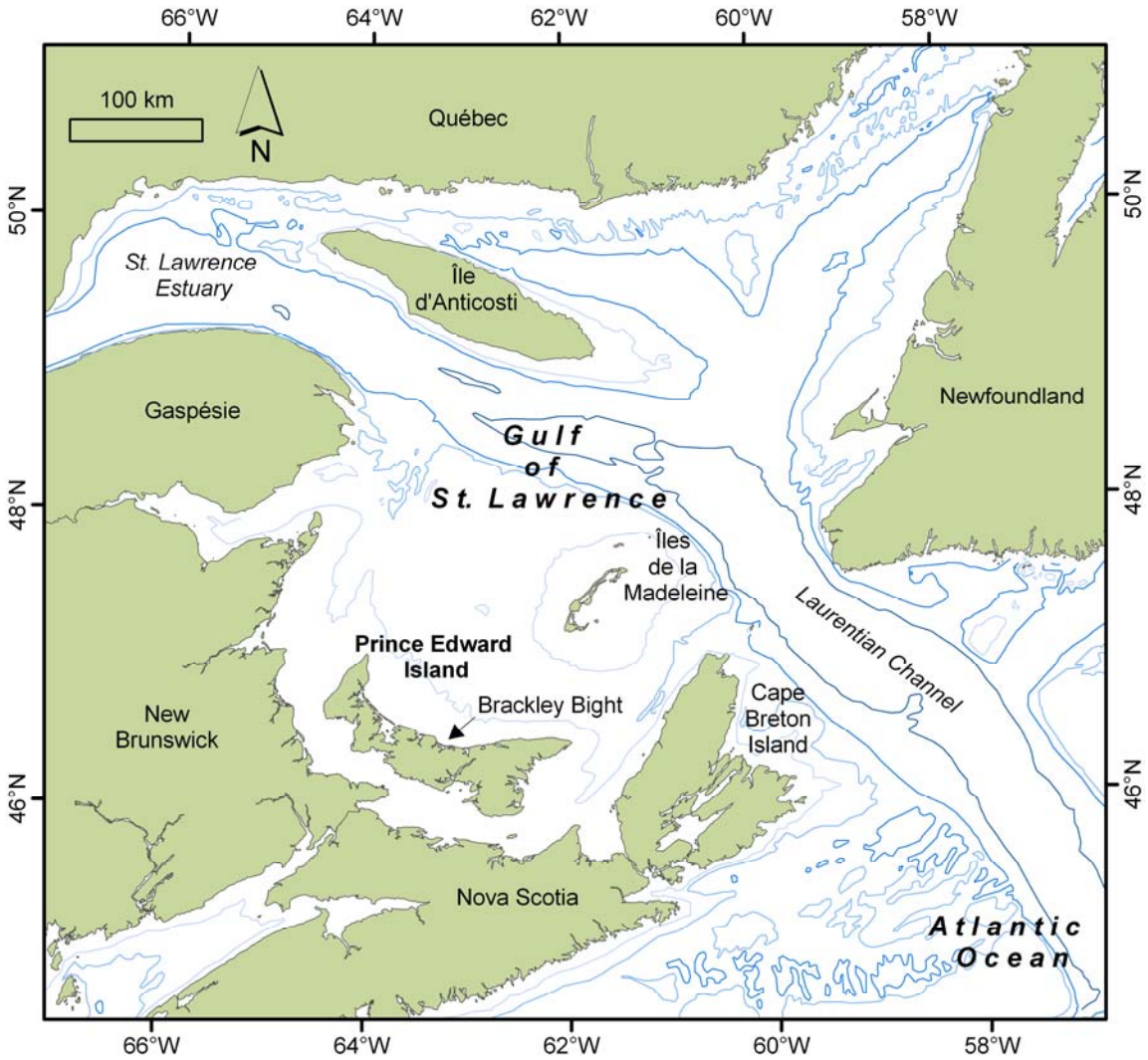

Figure 1. Location of the Brackley Bight study area in the southern Gulf of St. Lawrence with the 50, 100, 200 and 400 m bathymetric contours.

The purpose of this paper is to describe the development of the configuration of the hydrodynamic and sediment transport model Mike21 that reasonably simulates nearshore waves, currents and sediment transport under autumn (i.e. ice-free) storm conditions while optimising run time. This research uses data collected during a sediment transport experiment in the autumn of 1999 as well as previous initiatives to map the nearshore of the Brackley Bight area and understand regional shoreline processes. Relevant previous fieldwork, both marine and terrestrial, will be described, followed by a brief description of Mike21 and the steps required for developing a successful configuration. The sensitivity of the Spectral Wave (SW), Hydrodynamic (HD) and Sand Transport (ST) modules to varying selected parameters in their setup will be described. For each module, a configuration is developed that best simulates storm waves, currents and sediment transport when compared to measurements and conceptual understanding of processes. This is the first step of a larger research project that will quantitatively investigate the potential impacts of changing climate on sediment transport in the Brackley Bight area and develop a methodology that can be applied in other regions, such as the Canadian Arctic, that may experience decreasing sea ice and changing storminess due to changing climate.

Previous Fieldwork

1999 Field Experiment (Hudson 99049)

A field experiment was conducted in Brackley Bight in the autumn of 1999 to measure waves and currents and gain insight into local sediment transport during storms. Two S4 combined current meters and wave/tide gauges were deployed in water depths of 4 m and 6 m, and a third instrument known as RALPH (Li and Heffler, 2002) was deployed in 13 m water depth (Fig. 2). The current and wave data from RALPH have not been processed, but hourly downward looking video recordings and sediment trap samples have been analysed. The S4s were first deployed on October 9, 1999 from MV Gulf Explorer and recorded currents hourly at 1 Hz in 15 minute bursts and waves hourly at 1 Hz averaged over 8.5 minutes (512 data points). The S4s were retrieved, downloaded and redeployed on October 17, 1999 and set to record every two hours rather than hourly to extend the length of deployment. The instruments were retrieved on December 19 1999. Similarly RALPH was deployed by CCGS Hudson on October 6, 1999 and retrieved, downloaded and redeployed on October 18, 1999 with final retrieval on December 19, 1999. In the first deployment, the burst camera recorded 25 s video bursts every 6 hours. The burst length was shortened to 14 s in the second deployment, still at 6 hour intervals.

Marine Surveys

Acoustic bathymetry was collected between 1997 and 2001, using a combination of singlebeam echosoundings from a Parks Canada rigid hull inflatable in Rustico Bay and Brackley Bay, Navitronics sweep multibeam in shallow waters from the PWGSC vessels Scotia Surveyor and Miramichi Surveyor, EM3000 multibeam in intermediate depths with CSL Plover and EM1000 multibeam in deeper waters from CCGS Frederick G. Creed. The EM1000 data includes backscatter, the strength of the return of the acoustic signal which provides information on seabed material. The acoustic bathymetry is further described in detail by Forbes and Manson (2002).

Acoustic bathymetry was supplemented with optical CASI (Compact Airborne Hyperspectral Imager) imagery. The technique for deriving bathymetry from CASI utilises the different attenuation rates of different wavelengths of visible light by water. As partially described by Morel (1996) and other unpublished works (cf. http://pws.prserv.net/RSP.4SM/), reflectance of pairs of image bands are compared and with several assumptions concerning attenuation coefficients, particularly the ratios of attenuation and resulting reflectance onshore and under water, bathymetry can be derived. The technique has been trialed on the north shore of PEI (Webster et al., 2002) and gives reasonable results to depths of approximately 5 m when compared to singlebeam echosoundings (Fig. 3).

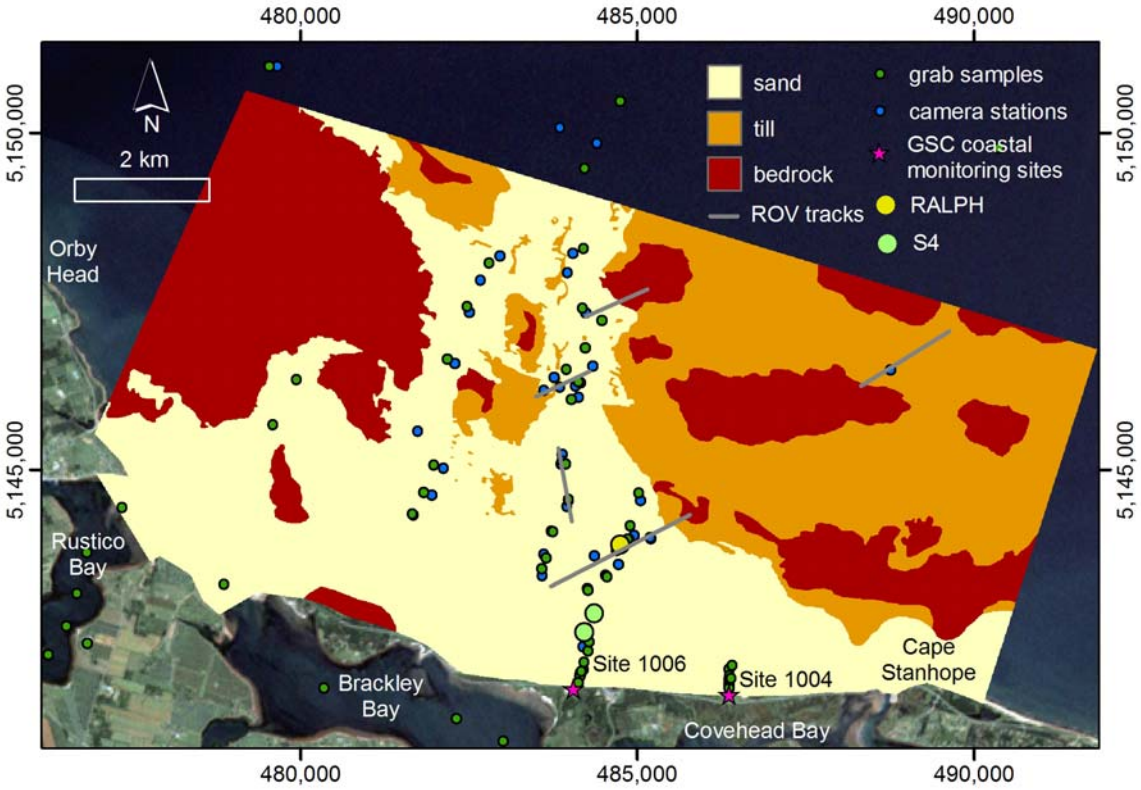

Figure 2. Sediment samples, camera stations, ROV tracks and the locations of RALPH and S4 deployments and the derived map of three interpreted seabed material classes in the domain. Also shown are some local place names and 2 key GSC coastal monitoring sites in the domain: from west to east, 1006 Brackley West (aka Covehead) and 1004 Brackley East. Coordinates in this and subsequent figures are UTM Zone 20.

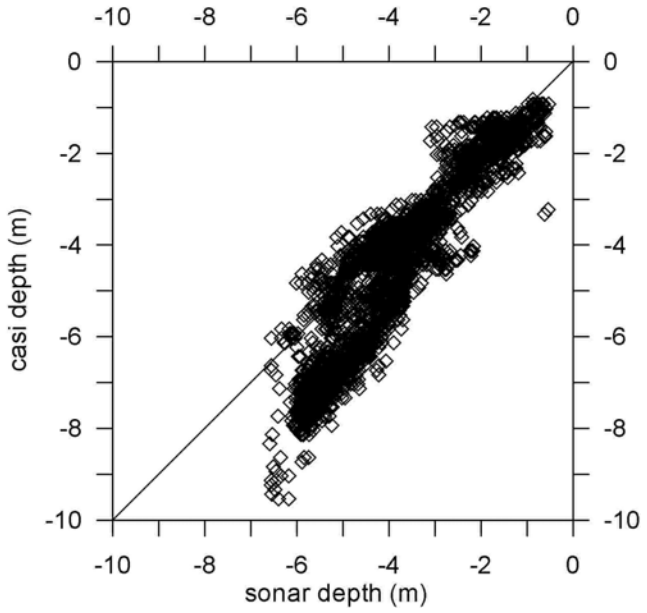

Figure 3. Comparison of depths derived from CASI with those from singlebeam echosounding showing reasonable agreement to approximately 5 m water depth. n=2656, r^2=0.85.

Further information on seabed conditions was obtained using drop cameras, grab samples and ROV (Remote Operated Vehicle) transects conducted in three cruises from 1998 to 2000 using CCGS Matthew and CCGS Hudson. Details on specific techniques are given by Forbes and Manson (2002). From the roughness in local bathymetry, presence of distinctive features (e.g. sand waves), acoustic backscatter, and the information obtained from the grab samples and imagery from drop camera stations and ROV transects, a map of generalised seabed sediment material classes and grain size distribution information suitable for input into Mike21 can be developed. Figure 2 shows this map, station locations and ROV/drop video camera transects. Three classes of seabed materials are mapped: fine rippled sand, cobble/boulder lag over till, and boulder lag over bedrock. For the sand class, the grain size analysis of grab samples returned the required statistics including d_{50} (mean grain size), d_{84} (84^{th} percentile of the distribution), and d_{16} (16^{th} percentile of the distribution) (Table 1). As is common in attempting to sample coarse materials, grab samples were not collected in the two lag material classes so drop camera and ROV imagery was used to estimate the required parameters (Table 1). From these, several other parameters are calculated including σ_g, the sediment grading coefficient, where $\sigma_g = \sqrt{d_{84}/d_{16}}$ (DHI, 2007), and, using published semi-empirical relationships, the Nikuradse coefficient k_s where $k_s \approx 2.5d_{50}$ (e.g. Soulsby, 1997) and the Manning number M, where $M=25.4/k_s^{1/6}$ (DHI, 2007).

Table 1. Attributes of the three interpreted seabed materials classes for Mike21 modelling.

Class	Description	d_{50} (mm)	d_{84} (mm)	d_{16} (mm)	σ_g	k_s (m)	M
1	fine sand, rippled	0.2	0.35	0.15	1.5	0.0005	90.2
2	pebble lag[a] over till	32	256	4	8	0.08	38.7
3	cobble lag[b] over bedrock	64	256[c]	32	2.8	0.16	34.5

[a] Pebble lag as defined here can contain material from granules to boulders of 256 mm
[b] Cobble lag as defined here can contain material from pebbles to boulders of 256 mm
[c] 256 mm is the largest grain size permitted in Mike21

Terrestrial Surveys

Terrestrial airborne LiDAR (Light Detection And Ranging) uses a laser to gather high density elevation points on land. The particular dataset used here was collected in August 2000 and is described in detail by Webster et al. (2002). However, one important difference between the LiDAR used in the analyses of Webster et al. (2002) and that used here is that Webster et al. (2002) derived a grid from the ground only returns. The LiDAR grid used here is derived from the ground and non-ground returns (aka all hits). The classification of LiDAR returns to ground and non-ground is typically done by filtering for abrupt changes in elevation that occur between vegetated or built areas and bare ground; however, Webster et al. (2006) describe situations in a LiDAR collection from coastal New Brunswick where bare sand dune crests are misclassified as non-ground, and similar effects are noted in a more recent collection in Halifax, Nova Scotia. This misclassification is also seen in the PEI LiDAR data at Brackley Bight (Fig. 4) which also demonstrates overestimation in marram grass behind dunes in the all returns data. Based on the consideration that a small overestimation in vegetated areas landward of the foredune crest is preferable to gross underestimation of the dune height and scarp location and thus flooding extent, the combined ground and non-ground LiDAR grid has been used in the Mike21 modelling. RTK (Real-Time Kinematic) GPS surveys were used to validate the LiDAR and demonstrate the difficulties associated with using ground-only data in coastal applications.

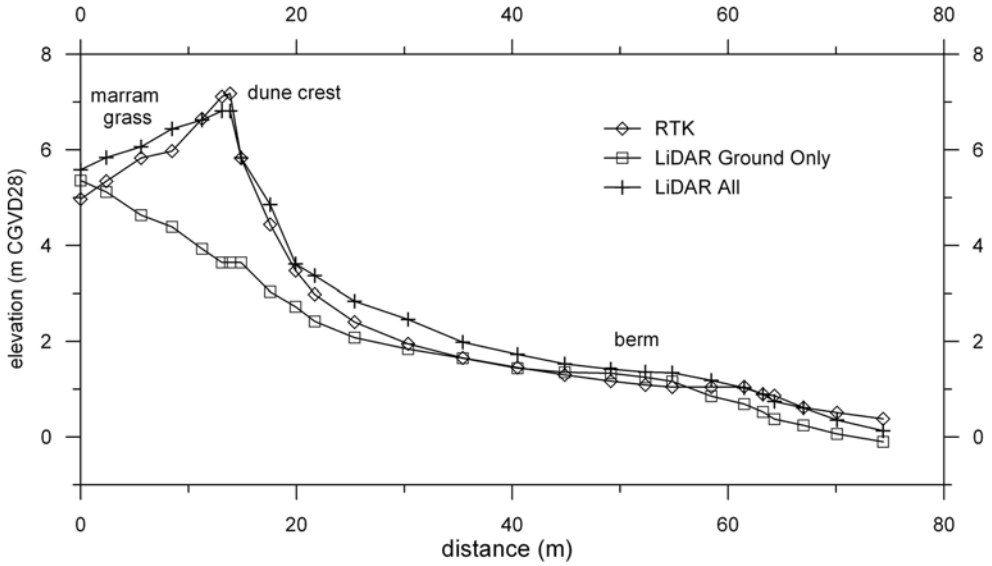

Figure 4. Comparison of RTK survey data with LiDAR ground and non-ground (aka all) returns showing the elimination of the dune crest in the ground-only classification and overestimation in the all returns data in marram grass behind dune. GSC site 1004 (Covehead), surveyed June 2000.

Configuration of Mike21

Mike21 FM (Flexible Mesh) is a commercially available dynamic coastal modelling software package developed and marketed by DHI (Danish Hydraulics Institute). It is modular in design such that different modules (in this case the Spectral Wave, Hydrodynamic, and Sand Transport modules) can be run simultaneously or separately. Simultaneously, each module runs at varying time steps depending upon the size of each mesh element, but provides updates to the other modules at a master time step. Separately certain outputs from the Spectral Wave (SW) and Hydrodynamic (HD) modules can be saved for input as required to subsequent runs of other modules, for example the Sand Transport (ST) module. To optimise run speeds for longer simulation periods, the master time step was set to one hour, though for the purposes of model configuration, a single storm over four days between November 30 and December 3 1999 was selected for simulation. Runs were conducted on a Dell PowerEdge™ 2900 server with 16 GB RAM and dual 3.16 GHz processors. For the domain and setup described herein, run times were approximately 15 minutes per simulated day.

Model Domain

Whether run simultaneously or separately, selected modules use the same domain. Construction of the domain requires a digital elevation model (DEM), a mesh, and defined boundaries.

DEM

A combined seafloor and land surface DEM was constructed from a combination of the acoustic and CASI bathymetry, and the terrestrial LiDAR described above. In order to prepare the DEM for input into Mike21, bathymetry was tide-corrected and converted to CGVD28 to match the LiDAR vertical datum. The datasets were merged at 5 m resolution with preference given first to acoustic bathymetry, then LiDAR, and finally to CASI bathymetry in depths shallower than 5 m. The merged DEM was resampled to 10 m resolution to smooth artifacts (e.g. tracklines and seams between datasets), and output as xyz points for import to Mike21 as scatter data. The DEM is shown coloured and hillshaded in Figure 5. Areas of missing data appear as the dark blue of the underlying satellite image.

Mesh and Domain Boundaries

The domain measures approximately 13 km alongshore and 7 km across-shore. It is defined by a northern quasi-shore-parallel boundary between 25 and 30 m water depth, and western and eastern quasi-shore-perpendicular boundaries connecting the northern boundary to a 4-segment land boundary broken by three inlet boundaries (Rustico, Brackley and Covehead; Fig. 5). These boundaries were digitized and defined in the Mike21 mesh generator, and a mesh was generated, smoothed, and interpolated to the DEM scatter data using linear interpolation to assign depths to nodes in areas of missing data. The last step in mesh generation is to refine the mesh to the bathymetry; through this process, mesh element areas were adjusted such that the areas of shallow elements were reduced and those of deeper elements were enlarged. The final mesh consists of 7148 triangular elements ranging in area from approximately 850 m^2 along the land boundary to 117,000 m^2 at the deepest part of the northern boundary (Fig. 5). Four profiles that will be discussed in following sections are shown, and their elevations from the input DEM and those derived during mesh interpolation are given in Figure 6. There is considerable generalisation of topography in water depths shallower than 10 m meaning that the model will not be able to resolve detailed processes in these depths. Given that the purpose of this model configuration is to reasonably accurately simulate relatively long time periods of sand transport within a coastal cell rather than precise replication of nearshore dynamics at a specific site, the computational efficiency obtained by larger nearshore mesh sizes is optimised.

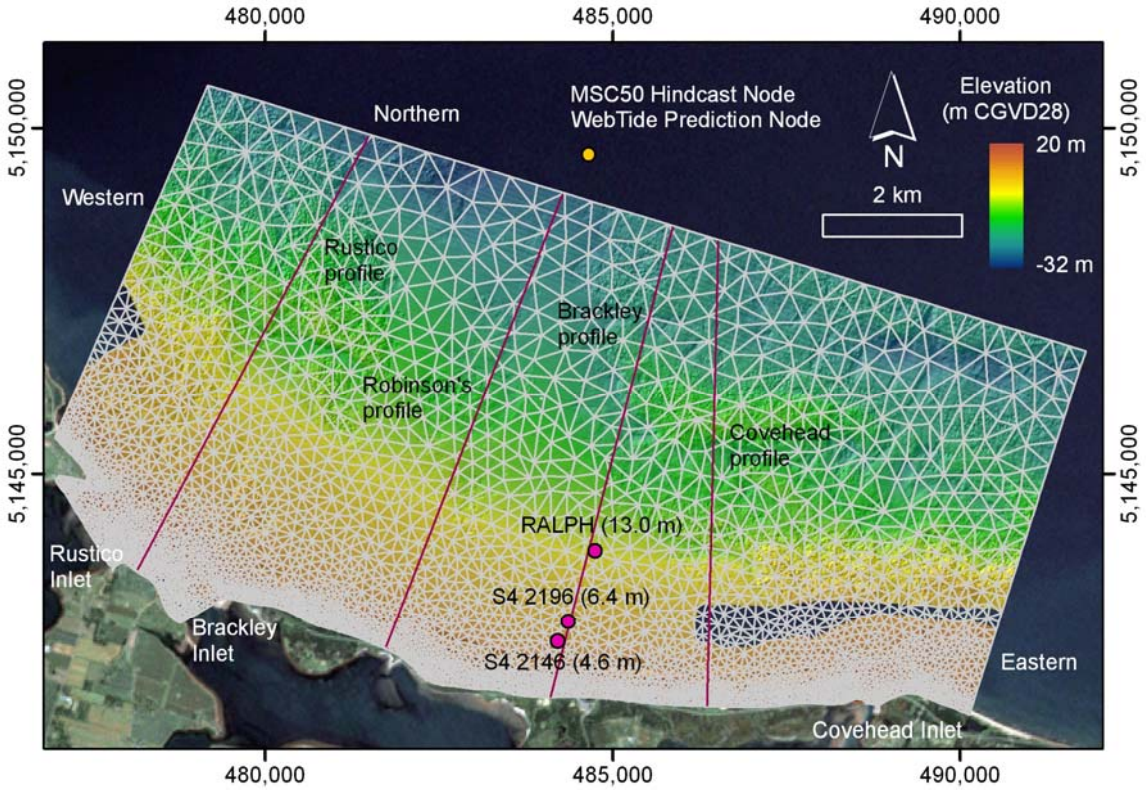

Figure 5. Model domain showing the input DEM and mesh, 3 ocean boundaries, and 3 inlet boundaries (the 4 land boundary segments are not labelled), and the MSC50 wave and wind hindcast node (coincident with the location of WebTide tide prediction node) used in the model. Also shown are the S4 and RALPH positions, and, in pink, the four profile lines. As labelled in figures following, these are, from east to west: Covehead, Brackley, Robinsons, and Rustico. The Brackley profile is roughly coincident with the 1999 instrument array.

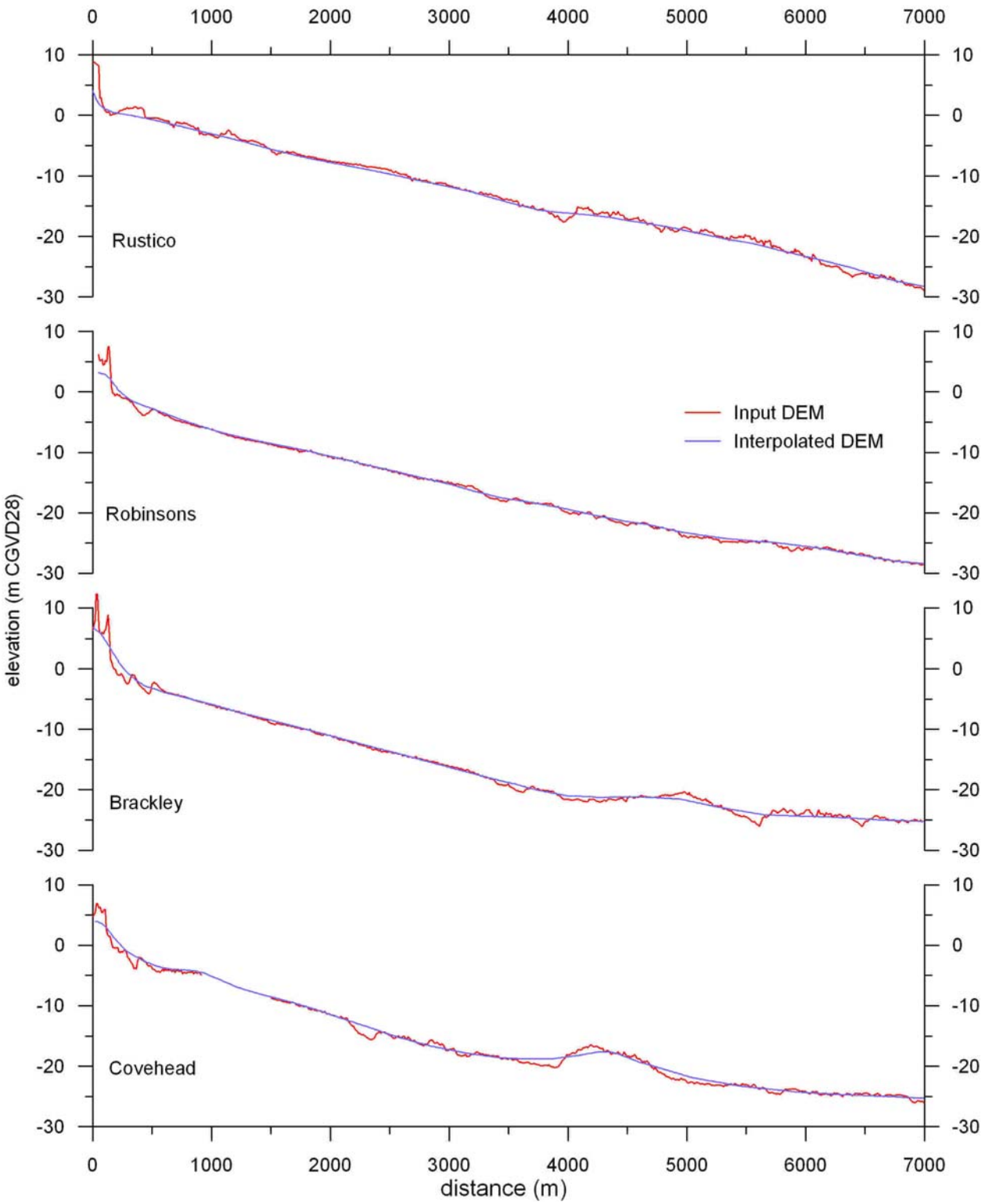

Figure 6. Comparison of profiles from the input DEM and the DEM interpolated to the model mesh.

Spectral Wave and Hydrodynamic Modules

The Spectral Wave and Hydrodynamic modules are typically run simultaneously as they feed back into one another at the selected master time step. For this reason, and because they share some similar or same inputs, they are considered here together. Figure 7 shows the inputs to the Spectral Wave and Hydrodynamic modules, their interactions, and outputs. These will be considered in turn and the module sensitivity to variations in some inputs will be explored.

Solution Techniques

For both modules, the basic equation options were chosen to optimise run time, accepting potential lower accuracy in results. For the SW module, the directionally decoupled parametric formulation was selected for the spectral equations and the quasi-stationary formulation for the time formulae using the low order, fast algorithm Newton-Raphson iteration solution technique with default parameters. Similarly the solution technique for the HD module was selected as lower order, and fast algorithm in both time and space with values for minimum and maximum time steps of 0.1 s and 20 s, and the critical CFL (Courant-Friedrich-Levy) number of 0.8. Other options in the SW module were accepted as the defaults, and current interactions from the HD module were not included as the model would consistently destabilize. Water levels were determined by the HD module and other options in the HD model were also accepted as default.

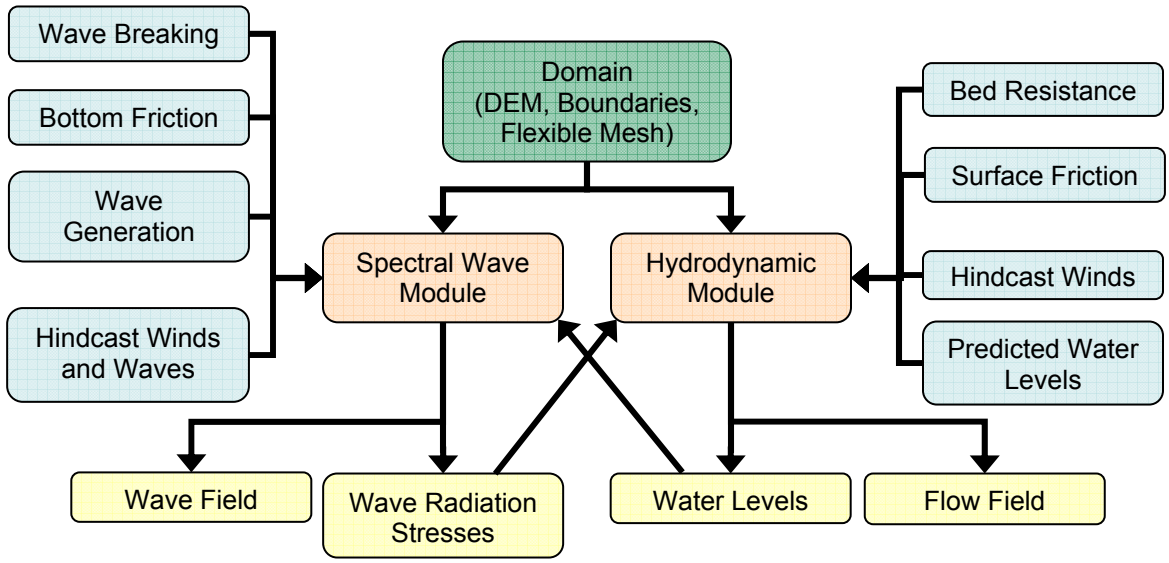

Figure 7. Inputs to, interactions between, and outputs from the Spectral Wave and Hydrodynamic modules of Mike21 when run simultaneously.

Boundary Conditions

The SW module was driven at the northern boundary by significant wave height, peak period, mean wave direction and directional spreading index from the MSC50 wave hindcast (Swail et al., 2006) obtained from the Meteorological Service of Canada. This hindcast consists of hourly wind and wave statistics from 1954 through 2005. Node M6010491 lies just outside the model domain (Fig. 5). The western and eastern boundaries were defined as lateral boundaries to which a one-dimensional transformation is applied from the northern boundary to zero at the dynamic water line. The three inlets were defined as closed such that no waves enter the domain and outgoing wave energy is fully absorbed (DHI, 2007).

Predicted water levels provided by WebTide, a regional tide and tidal current model developed by Fisheries and Oceans Canada (Dupont et al., 2002), were chosen to drive the HD module. It is necessary

to use predicted tides because, after removal of the Rustico gauge in 1996, there is no tide gauge operating on the North Shore of PEI. The intention is to model time periods without measured tide data, so, though the 1999 field experiment deployed S4 current meters measuring water levels, predicted tides are used and the measurements are compared to the model results. WebTide water levels were determined for the same location as the MSC50 wind and wave hindcast node. Attempts were made to run the model with WebTide currents as boundary conditions but these were less successful in generating storm driven water levels and the overall model stability was reduced.

Hindcast Winds

Both the SW and HD modules require hindcast wind inputs. MSC50 hindcast wind speed and directions from the same node as the hindcast waves were used as these inputs. For the HD module wind friction was allowed to vary with wind speed as per the Mike21 default; for the SW module several tests were conducted to determine the best formulation for wave generation by winds, and will be discussed in a following section.

Wave Breaking

DHI (2007) suggests that the parameters for wave breaking in the SW module can be varied to calibrate model results to field measurements. The formulation of Ruessink et al. (2003), applicable to barred and planar beaches, includes two parameters: α, a proportionality constant, and γ, a wave height-to-depth ratio related to local wave number. The defaults of α=1 and γ=1 were found to under-predict wave height. Increasing the values of α and γ to 2 improved prediction, but higher values again resulted in under-prediction of significant wave height. Varying the wave breaking parameters had negligible effect on peak wave period. Values of 2 for α and γ appear optimal in predicting significant wave height (Fig. 8).

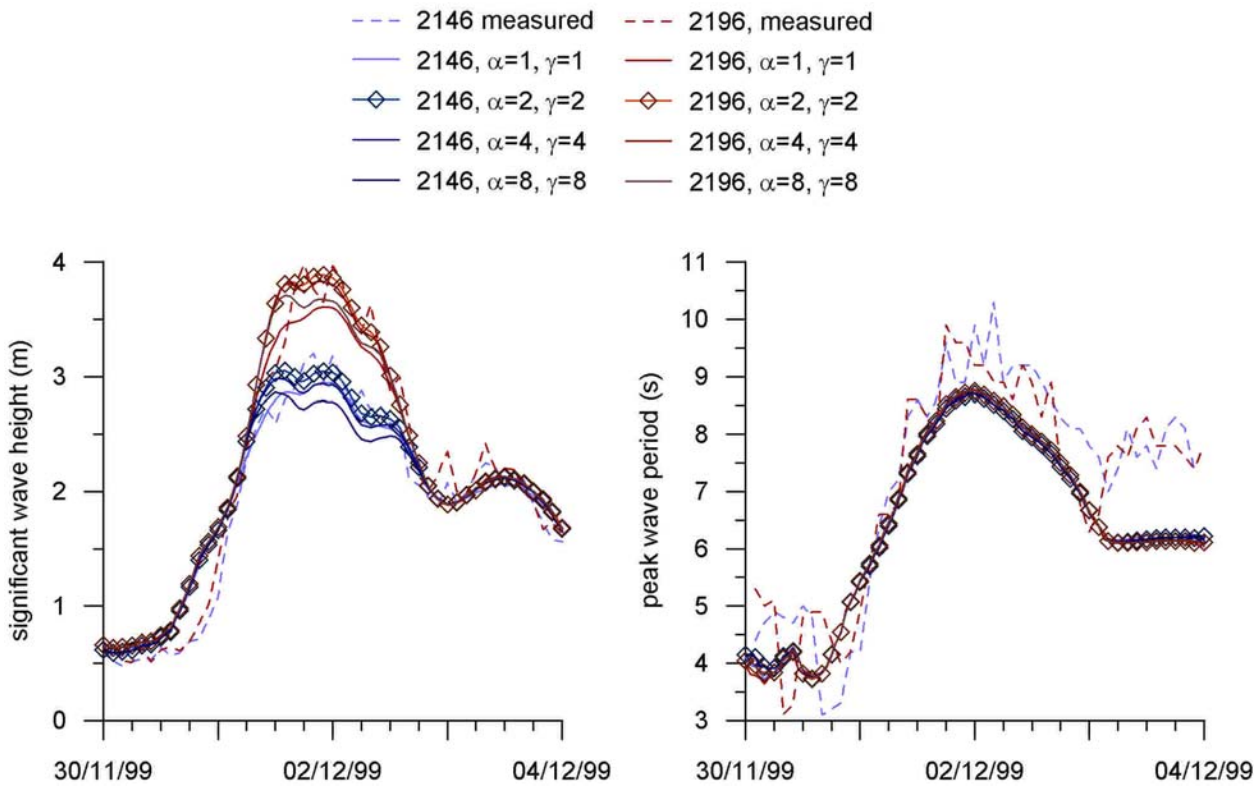

Figure 8. Effects of varying wave breaking parameters on the predicted significant wave height and peak period. Symbols represent optimal configurations. 2146 and 2196 refer to the two S4 instruments (see Fig. 5).

Wind Forcing

Figure 8 shows reasonable prediction of significant wave heights, yet continuing under-prediction of peak periods. Mike21 offers several choices of formulations for generating waves from winds including JONSWAP (Hasselmann et al., 1980), Kalma and Calkoen (1994), SPM73 and SPM73 (USACE, 1973), SPM84 (USACE, 1984) and SPM73/HBH (Holthuijsen et al., 1989; USACE, 1973). Johnson (1998) investigated these different formulations and found significant differences between them achieving most success with JONSWAP, Kahma and Calkoen (1994) and SPM73 with coefficients from Holthuijsen et al. (1989) (i.e. SPM73/HBH). Figure 9 shows that the choice of wind forcing formulation makes some difference to predicted peak wave periods in the Brackley Bight study area with the SPM73 best approaching the S4 measurements, however all formulations result in over-prediction of significant wave heights as storm winds grow and diminish; the effect is smallest with the JONSWAP formulation. All formulations produce similar results at the storm peak. To best simulate wave heights during storm waxing and waning while reasonably simulating peak periods, the JONSWAP formulation (default in Mike21) appears optimal likely in part due to its use of 10 m elevation winds equivalent to the MSC50 hindcast, and widely accepted use in fetch restricted but deep waters such as are found in the central Gulf of St. Lawrence (DHI, 2007; Johnson, 1998).

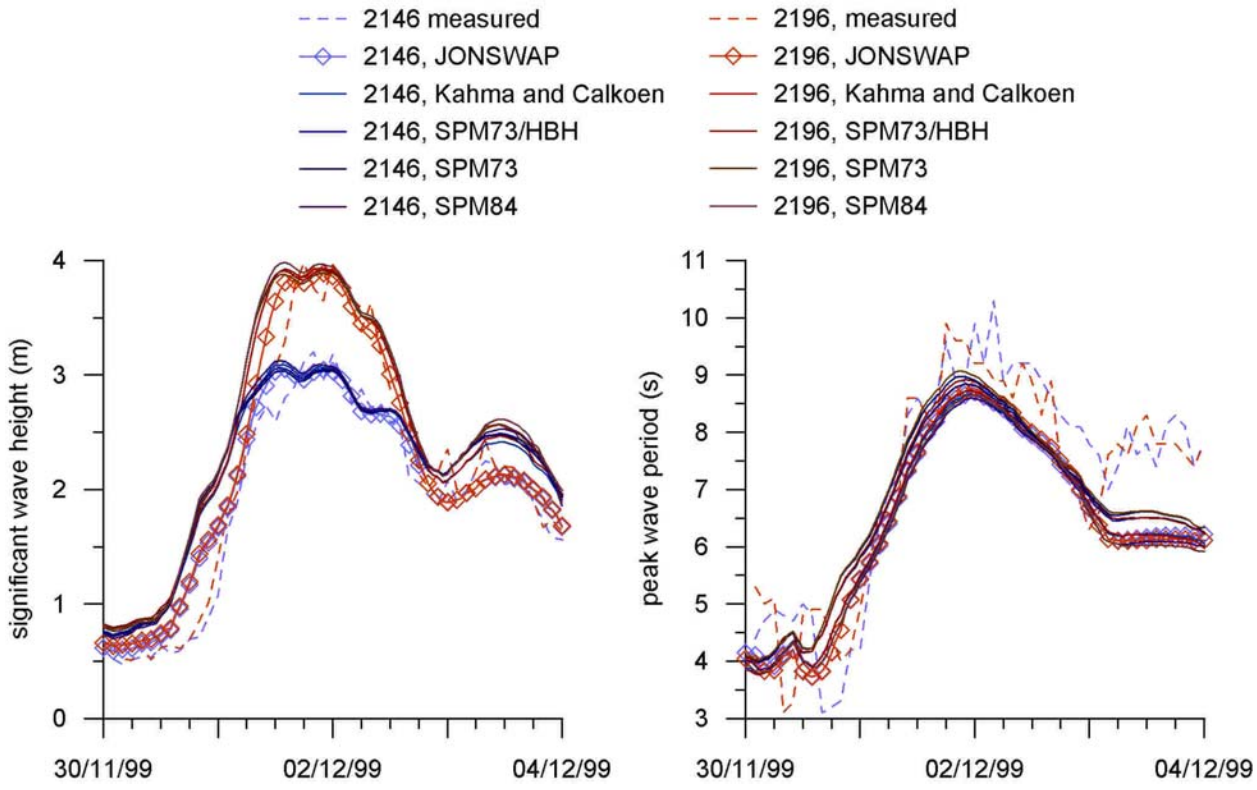

Figure 9. Effects of varying wind forcing formulation on the predicted significant wave height and peak period.

Bottom Friction and Bed Resistance

Bottom friction is represented in the SW module by the Nikuradse coefficient k_s as described above. The HD module requires a similar and related parameter, the Manning number M, also described above. DHI (2007) suggests that values of k_s and M can be altered to calibrate the model. Recommended values from Soulsby (1997) include $k_s = 2.5d_{50}$ (Table 1), but it was found that while using this value for k_s results in reasonable prediction of wave height, wave period is underpredicted (Fig. 10). Other values larger and smaller than this were tested with a reasonable value of $k_s=d_{50}$. Considering that maintaining the theoretical relationship between ks and M might contribute to model stability, values of M were varied

accordingly (Fig. 11). Current speeds in the HD module are also sensitive to varying M and the value of M corresponding to $k_s=d_{50}$ was found to give reasonable results for current speed. Note that in Figure 11 and subsequent figures showing current speeds from the S4 instruments, speeds at the instrument height (0.6 m above the seabed) have been converted to depth-averaged current speeds $\bar{U}$ following Soulsby (1997, rearranged from Equ. SC34)

$$\bar{U} = \frac{7u_*}{\left(\frac{d_{50}}{h}\right)^{1/7}}$$

where u_* is the measured current at height h above the seabed. This allows comparison to $\bar{U}$ output by Mike21. The results for current speed show slightly higher currents at the outer S4 (2196) than the inner S4 (2146) which is opposite to what the measurements show. No model configuration resolved this relatively minor error which may be related to differences in bathymetry during the field experiment (when nearshore bars were present) and the bathymetry represented in the model in which mesh generation smoothed bar morphology. Water levels from the HD module are insensitive to varying M and require additional calibration to correct their general under-prediction (Fig. 11).

Wind Friction

Wind friction coefficient in the HD module is another variable that can be adjusted to calibrate Mike21 (DHI, 2007). The results of varying wind friction coefficient are shown in Figure 12. Both current speed and water level are sensitive to varying wind friction coefficient. Higher values of wind friction coefficient (0.004) raise water levels to approximate the measurements at the S4 current meters, however the use of the Manning number of 0.4M (where M is the Manning number in Table 1) resulted in overestimation of current speeds. With the optimal wind friction coefficient of 0.004, a slightly lower value of 0.35M was adopted, resulting in a slight over-prediction of current speeds at the outer S4 (2196) and good prediction at the inner S4 (2146).

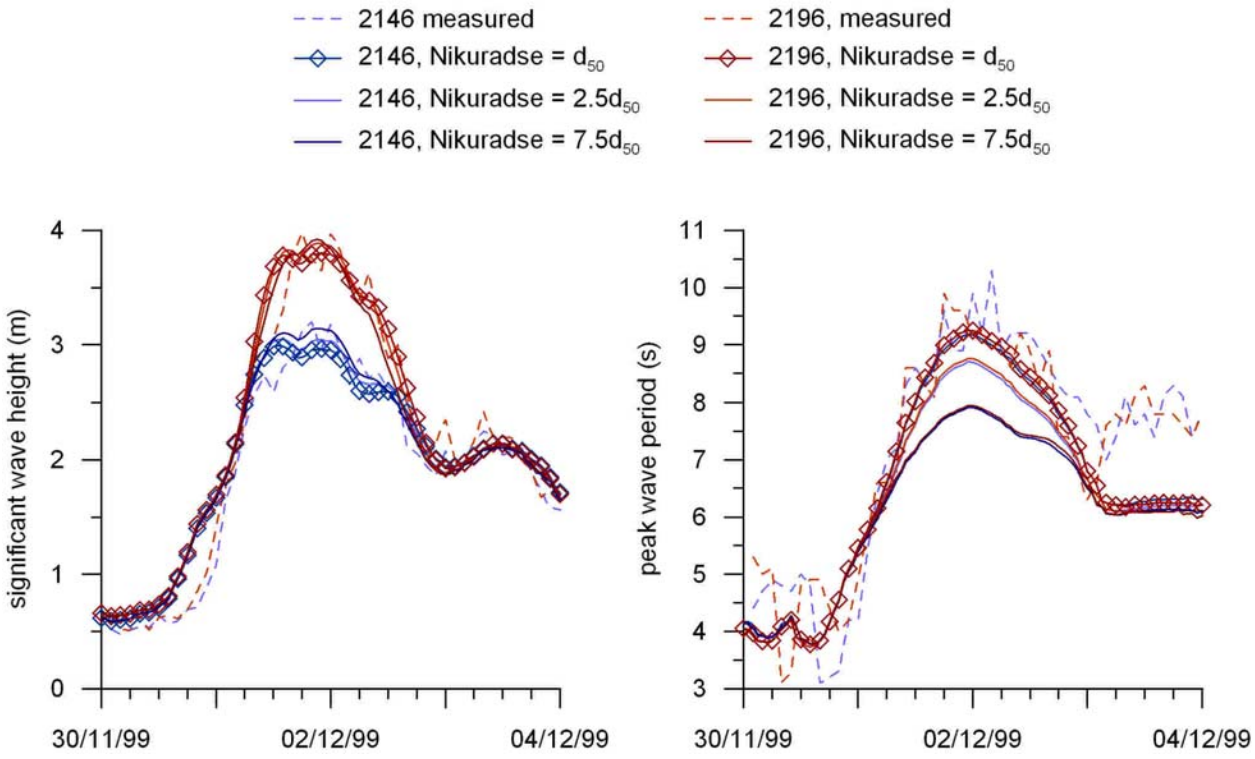

Figure 10. Effects of varying Nikuradse coefficient on significant wave height and peak period. The optimal coefficient appears to be $k_s = d_{50}$.

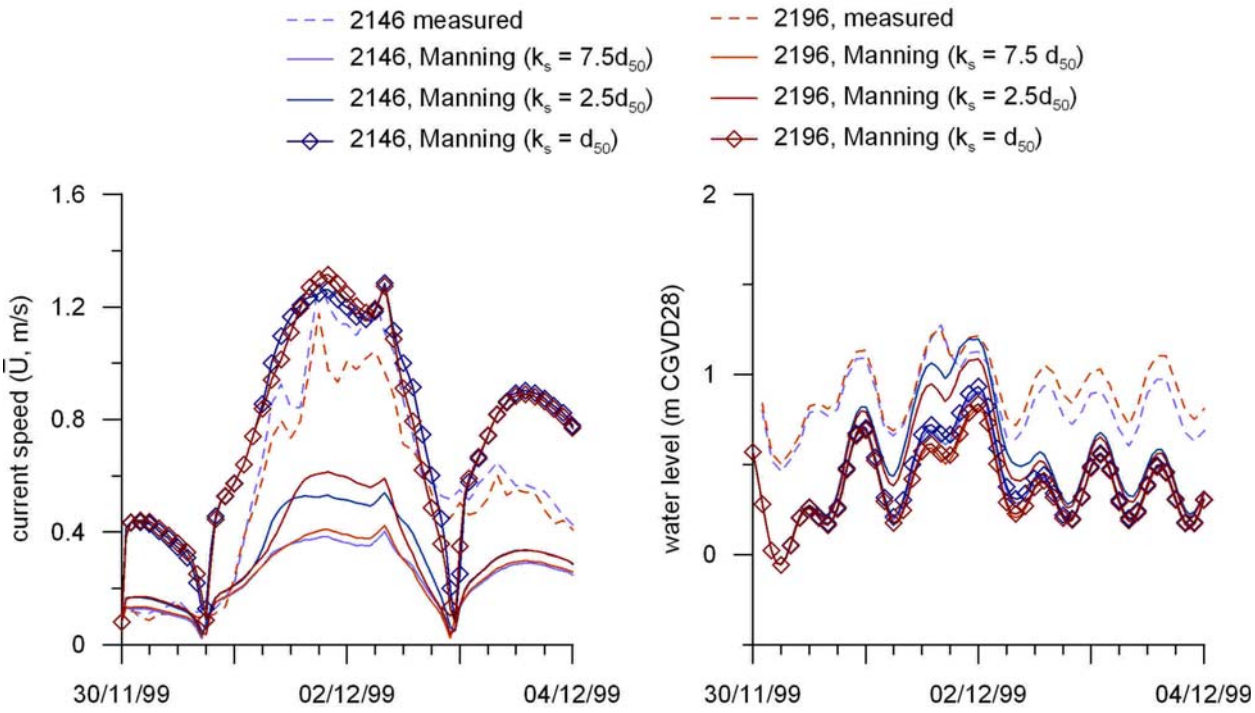

Figure 11. Effects of varying Manning's M on depth-averaged current speed and water level. Reasonable results are obtained using a value of M corresponding to $k_s = d_{50}$.

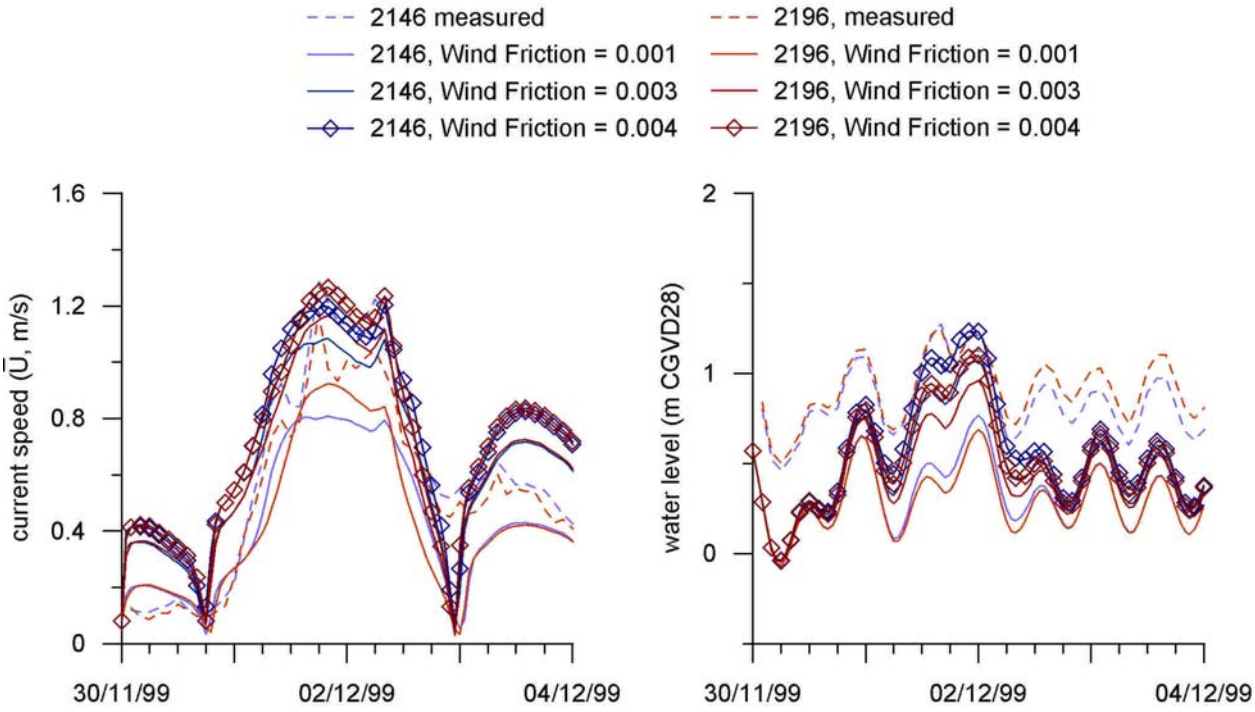

Figure 12. Effects of varying wind friction coefficient on depth-averaged current speed and water level, with an adopted Manning number corresponding to $k_s = d_{50}$.

Sand Transport Module

The ST module itself is relatively simple requiring only grain size and layer thickness information, the domain used in the HD and SW modules, and outputs from those two modules (Fig. 13). However it has two sub-components, STPQ3D and the Morphology Module, which require a number of items and considerable a priori knowledge of conditions in the domain.

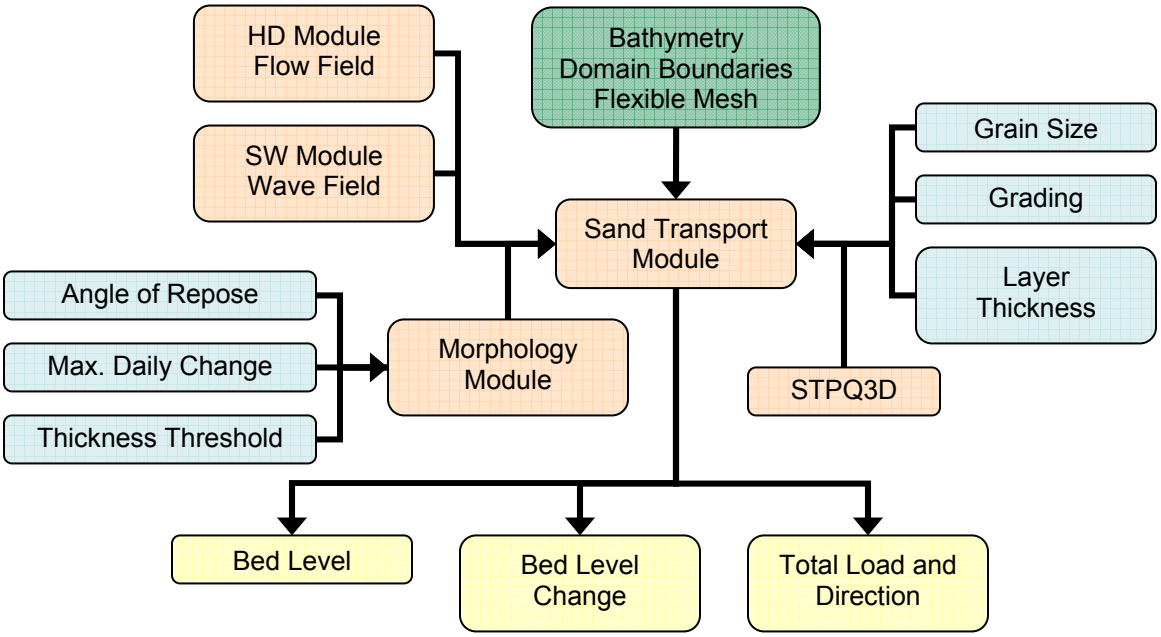

Figure 13. Schematic of inputs to, and outputs from, the Sand Transport module.

Layer Thickness

Sub-bottom profiling conducted between 1999 and 2001 gives thickness of the mobile bed (layer thickness) and reveals complex topography of glacial sediments and bedrock related to channels of former rivers that flowed across the now inner continental shelf to the former shoreline. These were subsequently buried under shoreface sands during transgression (Forbes and Manson, 2002). For the purposes of modelling sediment transport over a few days and even years, detailed sediment thickness related to sub-surface topography beyond a few metres below the seabed is not required. Indeed, RALPH video shows storm wave-induced erosion of a rippled sandy bed to an underlying stable cobble lag. For simplicity, based on core penetration and drop camera and ROV imagery, a single value for bed thickness has been adopted for each seabed material class: 2 m for sand, 1 m for lag over till, and 0.5 m for lag over bedrock. This input layer was then mean-filtered to avoid model instability due to abrupt changes in layer thickness.

STPQ3D

STPQ3D is a sediment transport program run in advance of the ST module. It uses a priori knowledge of conditions in the domain to calculate expected sediment transport rates in the along- and across-shore directions. It is a sub-program used to generate sediment transport look-up tables and, in essence, determines the suspended sediment concentrations; the ST module merely controls the time step, and with

the other modules the transport rate and direction, and the outputs. General parameters in STPQ3D include the tolerance in sediment concentrations, the number of wave periods, steps per period for which to populate the tables, relative sediment density, critical Shields parameter, and water temperature. Additional parameters allow for inclusion or exclusion of ripples, bed slope, streaming, density currents, centrifugal acceleration and choice of whether bed concentration is calculated by deterministic or empirical formulae. Wave parameters allow the selection of a wave theory and values of wave breaking parameters, and the final step of STPQ3D is to define the sediment transport table axes including appropriate minima, maxima, and step value (i.e. resolution) for expected conditions in the domain.

Fourteen different configurations of STPQ3D were explored. In all configurations the general parameters were kept constant at their default values (tolerance=0.0001, number of wave periods=150 s, steps per period=140, relative density=2.65, critical Shields parameter=0.05 and water temperature=10^{o}C). Similarly, the wave parameters were also held constant using the theory of Doering and Bowen (1995) and, as recommended by DHI (2007), the breaking wave parameter values used equaled those in the SW module (both equal to 2). Some of the additional parameters were varied, as well as the sediment transport table axes time step values, and therefore the detail of the sediment transport table. Most STPQ3D configurations gave results difficult to reconcile with conceptual understanding of sediment transport in the study area and only a few selected configurations will be presented here as examples. These are a first complex case in terms of both secondary options and parameter detail (Case 1), and a second simple case in terms of both secondary options and parameter detail (Case 2) (Tables 2, 3, and 4). In tables 3 and 4, for all parameters (except grain size) the maximum value is obtained by adding the interval for the number of steps. For grain size, the maximum value is obtained through multiplication of the interval by the number of steps.

The results of Case 1 are shown in Figure 14 and Case 2 in Figure 15. In these figures the colours represent the amount of bed level change between t_0 and t_{96} (where t is the hourly model time step indicated by the subscript which ranges from 0 to 96 over the four day simulation), the arrows give the direction of transport at t_{42} (peak of storm), and the texture in the background is hill-shaded bathymetry differentiating the seabed classes. The main difference between Cases 1 and 2 is whether streaming (mass transport in the wave boundary layer) is included (other configurations showed the inclusion of bed slope made no apparent difference). Figure 14 shows abrupt changes in transport directions corresponding to changes in seabed class (labels A and B), whereas the effect is diminished in Figure 15. Figure 15 also shows development of more complicated circulation at C and D. Figure 14 shows that the maximum depth of deposition is less than that of erosion, whereas in Figure 15 they are balanced. Both show development of cell-like patterns of erosion and deposition alongshore.

Morphology Module

The morphology module is included in the ST module for studies that require morphological simulation. In contrast to the SW and HD modules for which quantitative measurements are available for calibration, the ST module calibration requires a certain level of conceptual understanding of nearshore processes and expected results.

Several different options were tested: boundary conditions, slope failure, maximum bed level change per day, sediment thickness threshold, and finally different definitions of the three sediment classes were explored. Boundary conditions include a choice between “zero sediment flux gradient” and “zero sediment flux gradient for outflow with no bed level change for inflow”. Runs were conducted to test the sensitivity of varying these but with no apparent differences; the “zero sediment flux gradient” option, essentially an open boundary allowing sediment transport out of the domain, and an infinite supply available for transport into the domain, was chosen as suitable for a sandy shoreline (e.g. Keen et al., 2003).

Table 2. Additional parameters in example cases of model runs investigating the sensitivity of sediment transport to configurations of STPQ3D.

Parameter	Case 1	Case 2
Inclusion of Ripples	Y	Y
Inclusion of Streaming	Y	N
Inclusion of Bed Slope	Y	Y
Inclusion of Density Currents	N	N
Inclusion of Undertow	Y	Y
Inclusion of Centrifugal Acc.	N	N
Bed Concentration	Deterministic	Deterministic

Table 3. Properties of sediment transport table axes for Case 1.

Axis	Start	Interval	Steps
Current Speed (m/s)	0.01	0.5	6
Wave Height (m)	0.1	1	8
Wave Period (s)	1	2	6
Wave Height/Water Depth	0.1	0.5	6
Angle Current/Waves (deg.)	0	30	12
Grain Size (mm)	0.06	4	8
Sediment Grading	1.1	2	6
Bed Slope in x and y (rad)	-0.5	0.5	3

Table 4. Properties of sediment transport table axes for Case 2.

Axis	Start	Interval	Steps
Current Speed (m/s)	0.01	1	3
Wave Height (m)	0.1	2	4
Wave Period (s)	1	5	3
Wave Height/Water Depth	0.1	1	3
Angle Current/Waves (deg.)	0	30	12
Grain Size (mm)	0.06	4	8
Sediment Grading	1.1	2	6

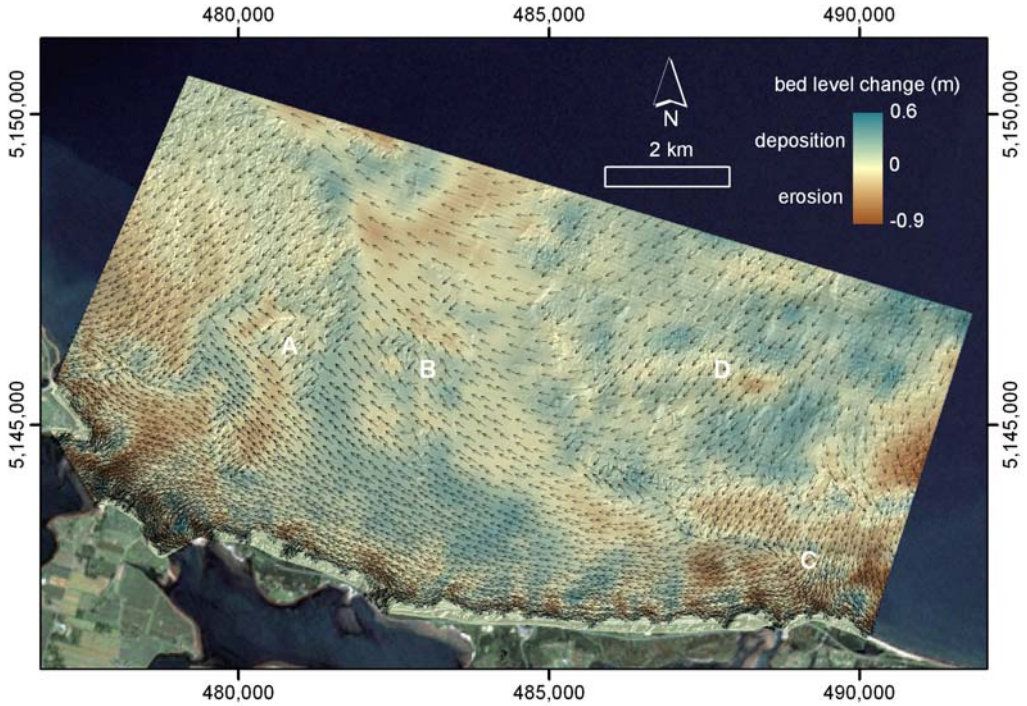

Figure 14. Case 1 bed level change from t_0 to t_{96} and sediment transport directions (arrows) at t_{42}, with shaded relief bathymetry showing abrupt changes in transport directions at changes in substrate and bed roughness (A and B) and a drift divide in transport directions at C. The hourly timestep is represented by t_h where the subscript h gives the hour.

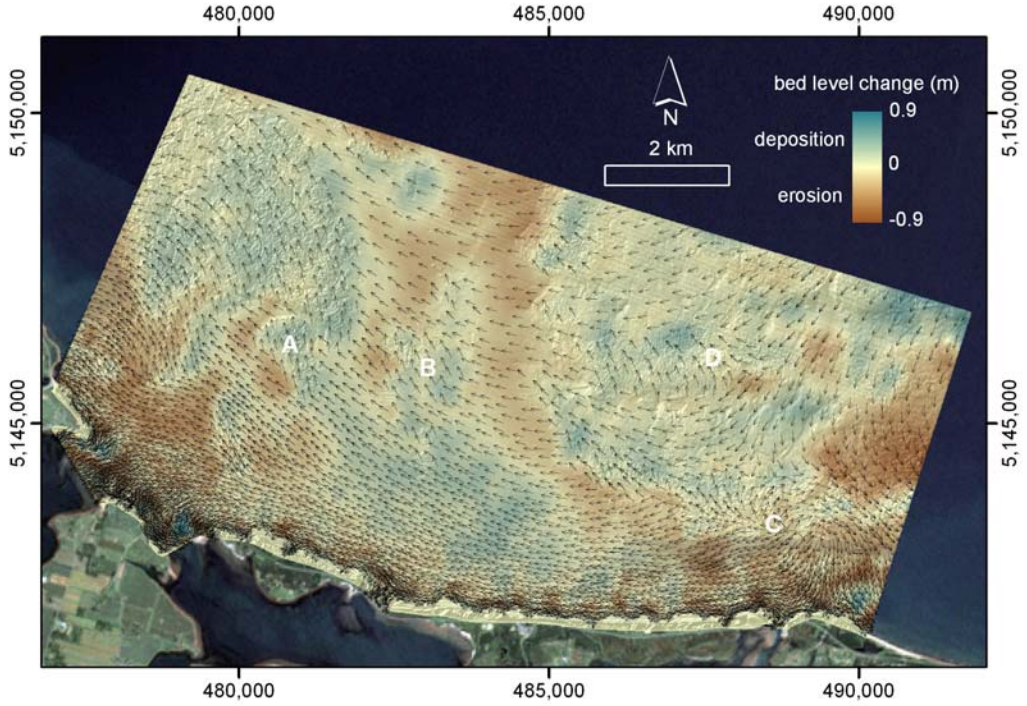

Figure 15. Case 2 bed level change from t_0 to t_{96} and sediment transport directions (arrows) at t_{42}, with shaded relief bathymetry showing smoother changes in transport directions at changes in substrate and bed roughness (A and B) and increased complexity in transport directions at C and D.

Slope failure was tested in three runs: one with no slope failure selected and two with slope failure and angles of repose of the default 32^o suitable for sands (Soulsby, 1997) and 70^o such as might be encountered with a recently scarped dune or berm. No apparent differences were found in the three runs when the four profiles at t_{96} were compared.

Another option is to vary the threshold thickness, which allows for a parabolic decrease in transport rate when the bed thickness is below a selected critical thickness (DHI, 2007). The default value of 0.1 m, and the values 0.25 m (approximately corresponding to cobble/boulder transition diameter) and 0.5 m (more typical of boulders in the domain) were tested. While the model is relatively insensitive to varying this parameter (Fig. 16), considering that sand will become trapped in the interstices between cobbles and boulders as currents rapidly decelerate with depth in the cobble or boulder layer, it seems reasonable to adopt the value of 0.5 m (corresponding to the approximate bed thickness of the boulder lag over bedrock class) as the threshold thickness under which transport decreases.

The module setup includes an arbitrary limit on the amount of bed level change per day. Values of 0.125 m, 0.25 m, and 0.5 m were tested. The model is highly sensitive to these small changes (Fig. 17). The number adopted as being reasonable to expect was 0.25 m/day. This is corroborated somewhat by downward looking video on RALPH which shows vertical changes estimated at about 15 cm during the modelled storm, which lasted about a day. Changes in shallower water can be expected to be larger than changes in deep water which is best shown in Figure 17 by the profile changes using a value of 0.25 m/day.

Revisiting the Sediment Class Definitions

Consideration was given to whether the interpretation of the ROV and drop camera imagery adequately estimated the amount of sand within the pebble and cobble lag deposits. Assuming that interstitial sand is present and mobile in these coarse deposits, the sediment properties of the two coarse lag classes in Table 1 were adjusted by decreasing d_{16} to lie within the fine sand range, thereby increasing the grading coefficient, and also reducing d_{50} to reflect a higher percentage of sand (Table 5).

In effect, this adjustment can be considered a warm start to the sediment transport module. With some sand available for transport in the otherwise immobile lag deposits, there is allowance for transport in and across these areas starting at t_1. Figure 18 shows that these adjustments in initial sediment conditions appear to eliminate the abrupt changes in sediment transport direction shown in Figure 14 and the complexity in sand transport directions shown Figure 15. The same configuration of STPQ3D given in Tables 2 and 4 (i.e. Case 2; Figure 15) was used in this simulation. Other tests using the Case 1 configuration (Tables 2 and 3 including streaming; Figure 14) demonstrated the same abrupt changes in transport direction, indicating that the ST module is sensitive to not only the STPQ3D configuration and the maximum amount of bed level change per day, but also to the initial definitions of the seabed sediments.

Table 5. Attributes of the three interpreted seabed materials classes for Mike21 modelling modified to include sand in the coarse lag classes, with k_s and M adjusted to reflect d_{50} rather than $2.5d_{50}$.

Class	Description	d_{50} (mm)	d_{84} (mm)	d_{16} (mm)	σ_g	k_s (m)	M
1	fine sand, rippled	0.2	0.35	0.15	1.5	0.0002	33.2
2	pebble lag[a] over till	20	256	0.2	35.7	0.02	14.3
3	cobble lag[b] over bedrock	50	256[c]	0.2	35.0	0.05	12.7

[a] Pebble lag as defined here can contain material from fine sand to boulders of 256 mm
[b] Cobble lag as defined here can contain material from fine sand to boulders of 256 mm
[c] 256 mm is the largest grain size permitted in Mike21

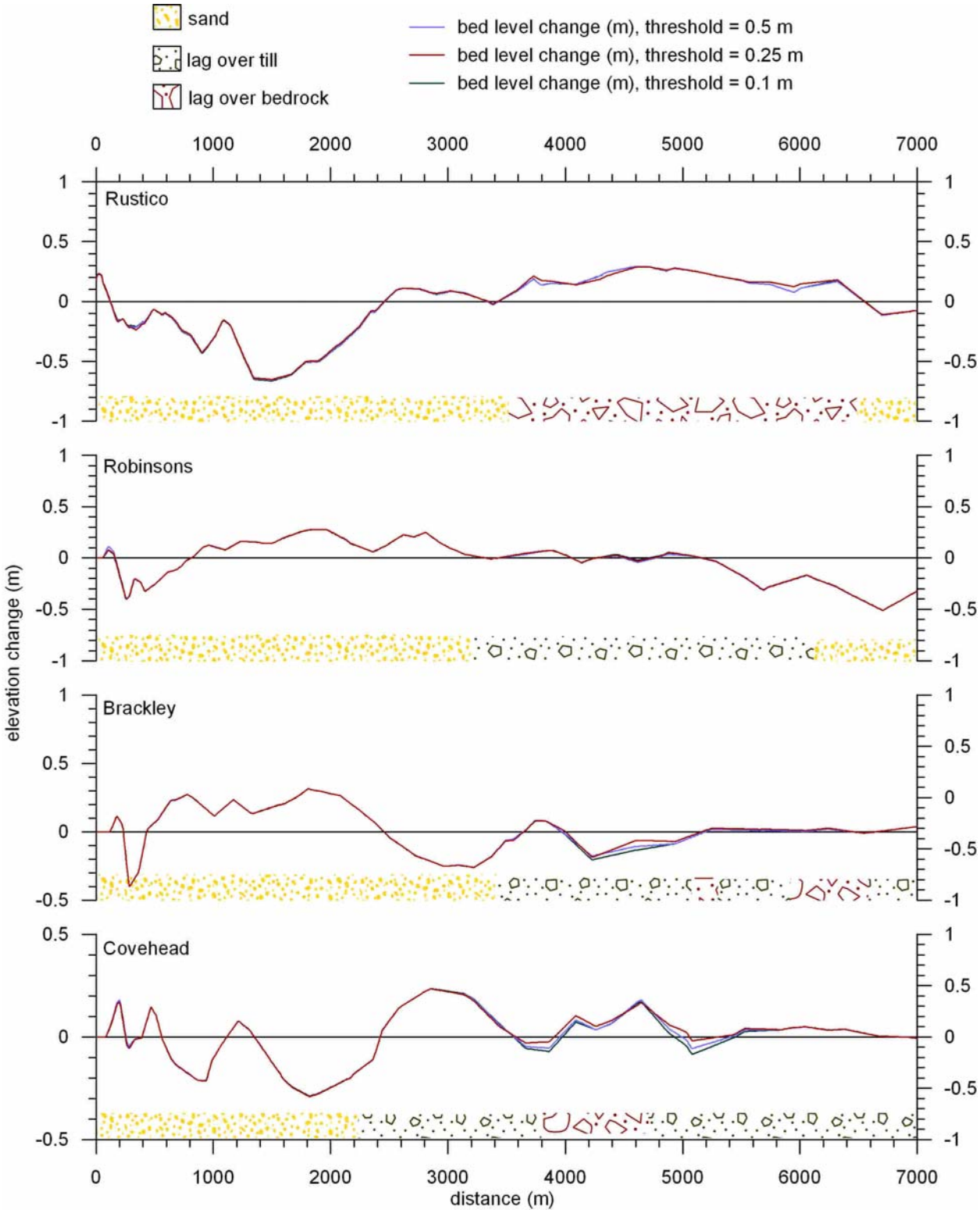

Figure 16. Results of varying the threshold thickness parameter. The value of 0.5, corresponding to the thickness of the boulder lag over bedrock sediment class seems reasonable to adopt.

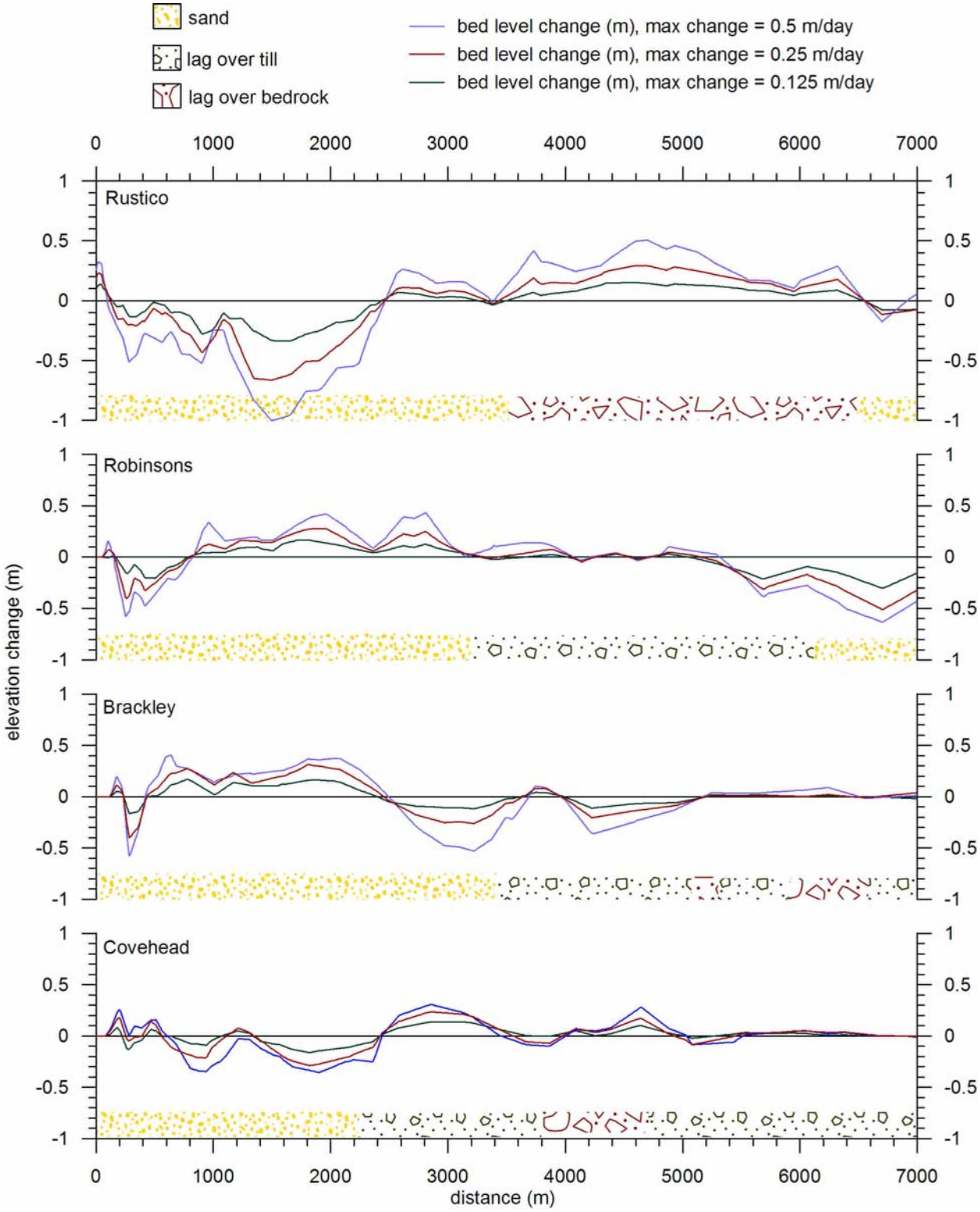

Figure 17. Results of varying the maximum allowable rate of change per day, showing the ST module is relatively sensitive to this parameter. The value of 0.25 m/day seems to give reasonable results.

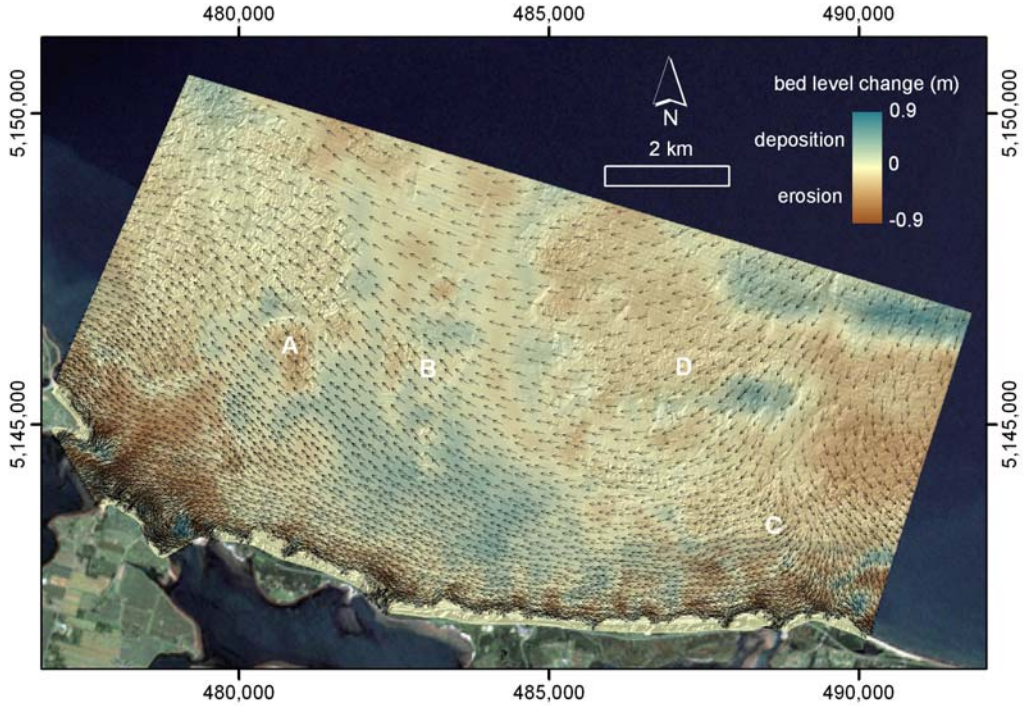

Figure 18. Bed level change from t_0 to t_{96} and sediment transport directions (arrows) at t_{42} as in Figures 14 and 15, but showing no abrupt changes in transport directions at A and B, and decreased complexity in transport directions at C and D. The drift divide at Cape Stanhope and sediment transport into Rustico and Brackley Inlets are accentuated.

Evaluation of the Adopted Configuration (Run28)

Based on the above experimental runs, a final configuration (termed Run28) was adopted with what appear to be optimal values for the tested parameters. Running the SW, HD, and ST modules simultaneously, these are: the DEM and domain as described above; the sediment classes as described in Table 5; wave breaking parameters α and γ both equal to 2; wind forcing using the JONSWAP formulation with a wind friction coefficient of 0.004; the Case 2 sediment transport table as described in the section on STPQ3D (Tables 2 and 4); zero sediment flux gradient boundary condition in the ST module; slope failure included with an angle of repose of 32^o; threshold thickness of 0.5 m; and the maximum daily amount of bed level change set to 0.25 m/day.

In Figure 19 are shown significant wave height and peak period modelled with the Run28 configuration and compared to the measured and input significant wave height and period from the MSC50 hindcast. Figure 19 demonstrates that the SW module predicts wave characteristics quite well, except for wave period at the end of the storm, which appears to be due to the input hindcast data. Linear regression gives correlation coefficients between measured and modelled significant wave heights and periods of 0.95 and 0.82 respectively and RMS errors of 0.24 m in significant height and 0.95 s in peak period (Fig. 20). Also shown in Figure 20 are the directional histograms of measured and modelled wave directions. Wave directions are also modelled well, though there is greater variability in modelled directions when compared to measured. Comparison of the modelled and measured data gives a circular regression coefficient of 0.73 and RMS error of 17.48 degrees.

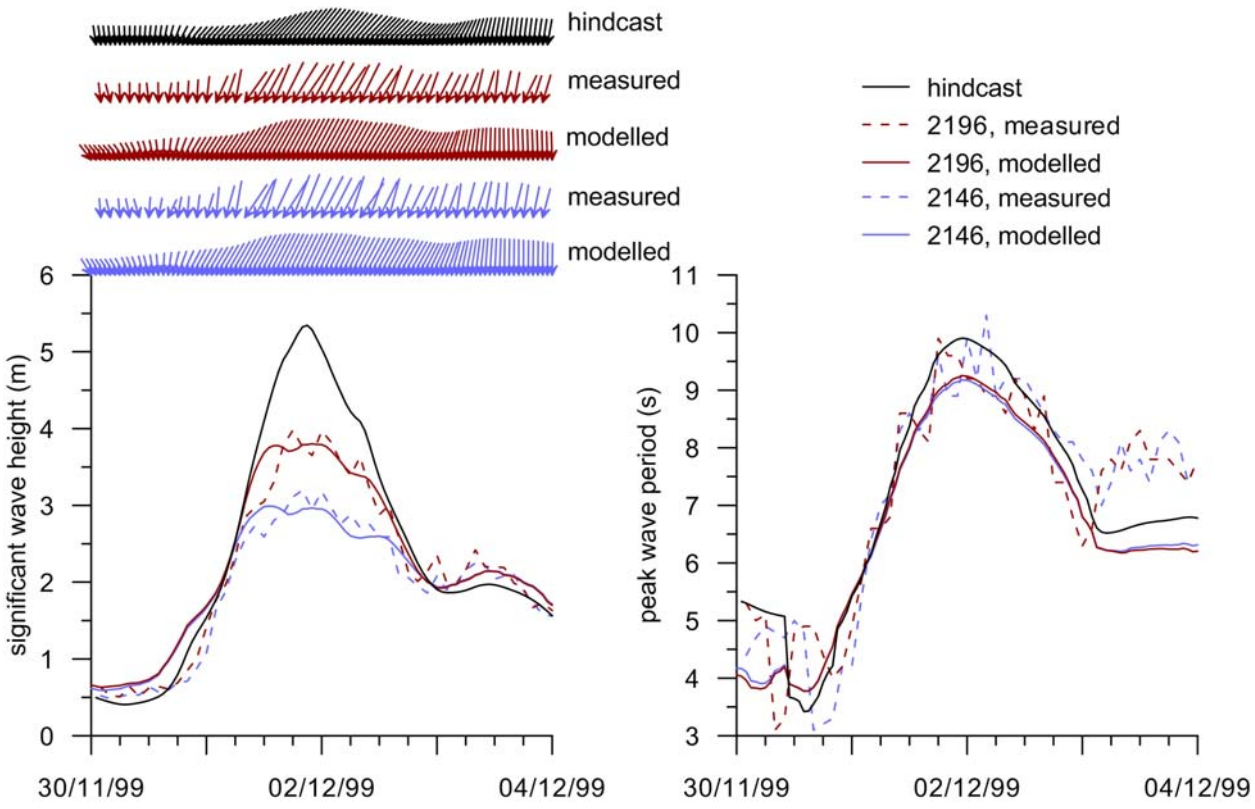

Figure 19. Results of the SW module in the final configuration, compared to the input hindcast and measured wave data. Top panel: vectors representing wave height and wave direction.

In Figure 21 are shown current speed and directions as well as water levels resulting from the HD module and compared to currents measured by the S4s. The results are less successful than those from the SW module. There are deviations in current speed at the beginning and end of the storm though speeds at the storm peak are reasonably well simulated. Modelled current directions show considerable alongshore alignment when compared to the measured results which have a stronger cross-shore component. There are also two prominent drops in modelled current speeds which correspond to reversals in current directions. These are near instant changes in the model results, suggesting that currents are simulated to drop to near zero during the direction reversal, whereas the measurements show a more gradual shift through north without an abrupt drop in speed, despite measurements being taken every two hours. The reason for this remains unclear, but may relate to the water levels which show similar patterns of anomalies during the beginning and ends of the storm. The storm peak itself is well-simulated.

The simulated water levels show initial underestimation relative to the measurements which were recording higher than normal water levels during consistent onshore winds through the field experiment. WebTide water levels used in the boundary conditions are predicted tides without any surge or setup effects so it is expected that the initial simulated levels are low. Low simulated water levels at the end of the storm are likely a result of modelling water levels over a small domain which does not incorporate larger phenomena outside the boundaries.

Correlations between modelled and measured water levels, current speeds, and directions are given in Figure 22. Water levels are correlated with an r^2 value of 0.64 and RMS error of 0.38 m. Current speeds are correlated with r^2 value of 0.79 and RMS error of 0.25 m/s. The circular correlation coefficient between modelled and measured current directions is 0.27 and the directions have an RMS error of 46 degrees.

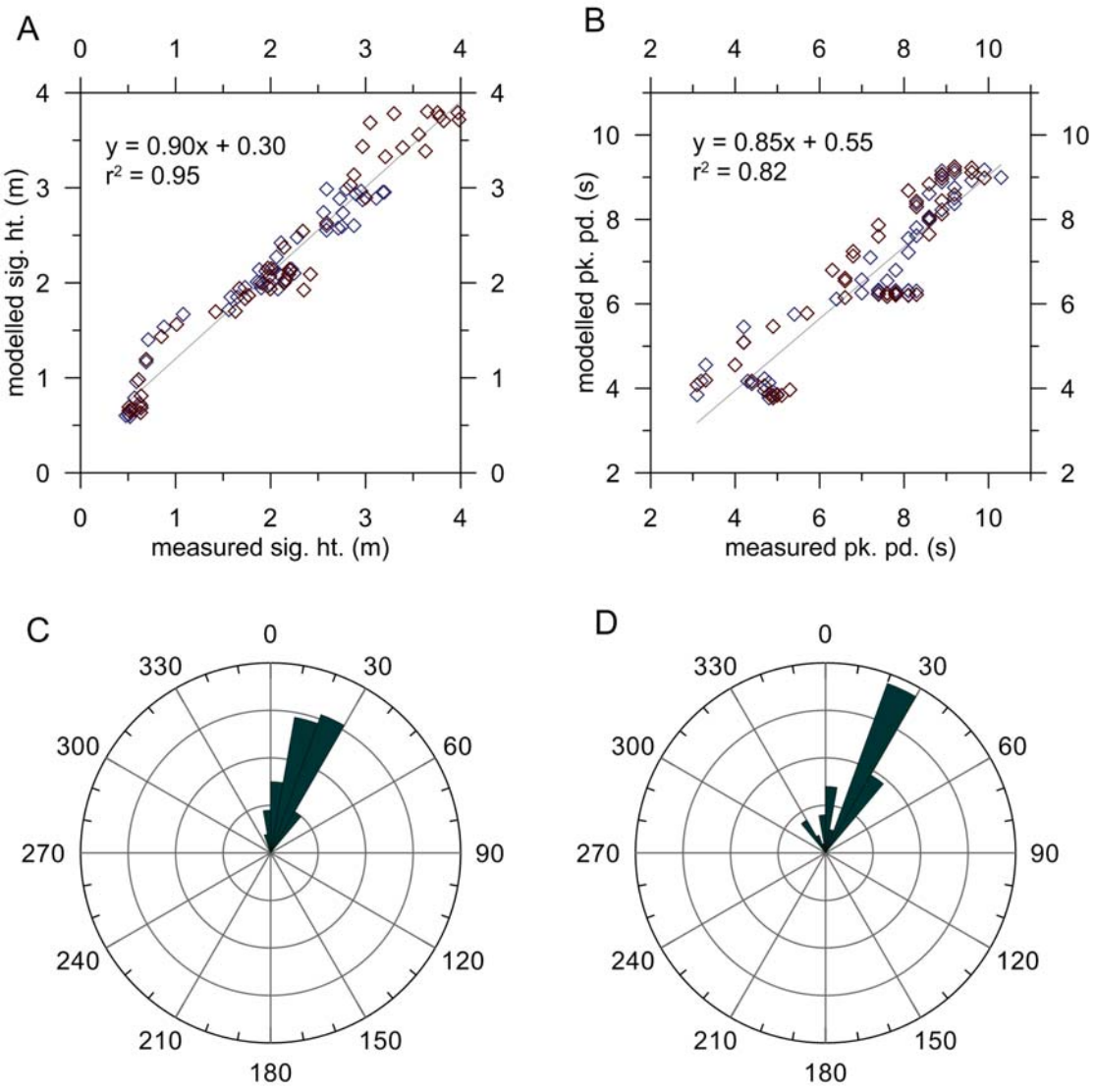

Figure 20. Correlation between measured and modelled significant wave heights (A), and peak periods (B), and the directional histograms of measured (C) and modelled (D) wave directions. Modelled and measured wave heights and periods are correlated with r^2 values of 0.95 and 0.82, respectively, and RMS errors of 0.24 m significant height and 0.95 s peak period. The circular correlation coefficient between measured and modelled wave directions is 0.73 with RMS error of 14.78 degrees. Rings are in increments of 10 samples.

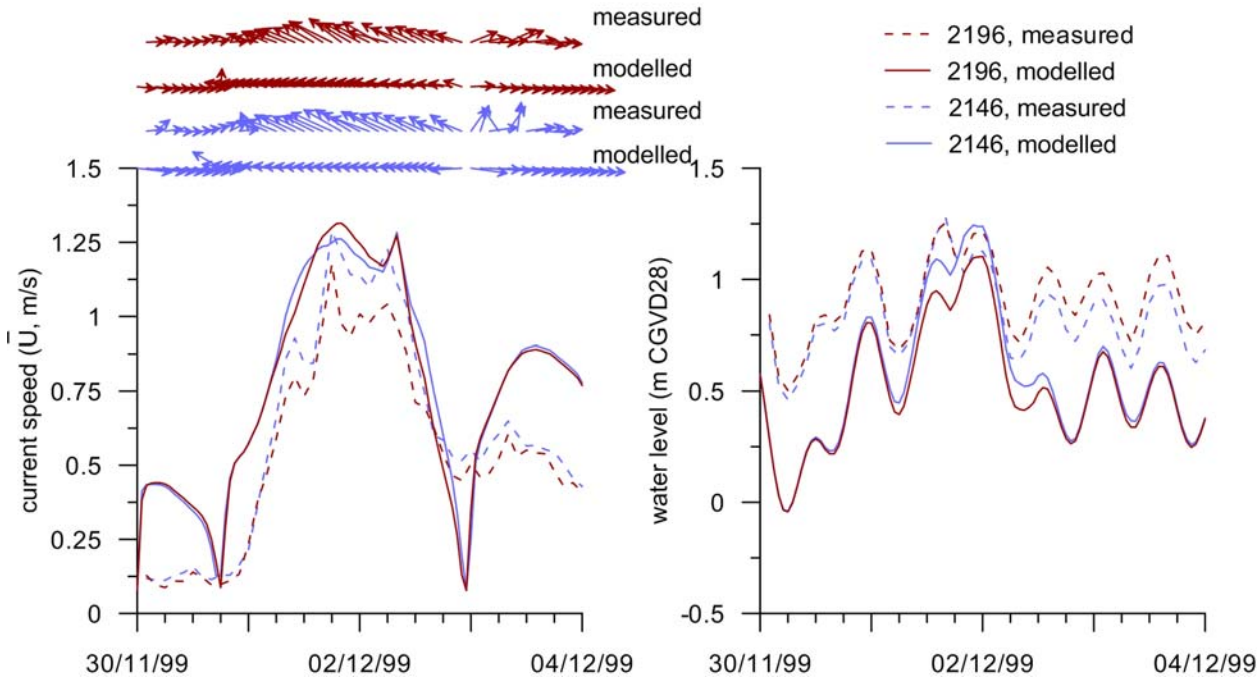

Figure 21. Results of the HD module from the final configuration compared to measurements from the S4 instruments. Top panel: vectors representing current speed and direction.

The dominant alongshore simulated current direction compared to the offshore directed component present in the measurements is likely contributed to by the depth-averaging of current direction in the model results as compared to current direction measured in the boundary layer (0.6 m above seabed) during the field experiment. In the boundary layer, it is expected that wave-driven currents dominate, whereas depth-averaged currents include a strong wind-driven component as well as a tidal component. Together, these may be directed more alongshore than the on- and off-shore oscillating flows under waves. Another contributor to the discrepancy may relate to more generalised bathymetric conditions in the model domain than during the field experiment (Fig. 6). If the instruments were located near topographic lows in bar crests that are not represented in model bathymetry, it is possible that the instruments were measuring off-shore directed flows not reproduced in the model.

In Figure 23 are shown the four profiles at t_0 and t_{96}, the elevation change, and the sediment classes across-shore. Overall, the profiles show a pattern of nearshore erosion and offshore deposition as would be expected from conceptual understanding and the amount of change appears to relate to depth and sediment class. The Covehead and Brackley profiles show this quite well with most changes occurring in the nearshore sands. The Rustico profile shows high erosion in the nearshore sands, and deposition in the offshore section of boulder lag. Figure 18 shows the erosion to be related to strong alongshore flows to the west, together with flow into Rustico Inlet. The deposition occurs as flow transporting sand from the infilled valley off Rustico Inlet to the east encounters the hydrologically rough boulder lag, and slows, thus depositing the eroded sand. The Robinson's profile shows relatively large changes (erosion) in deep water which appear anomalous. However, these changes occur in the sand class, and multibeam bathymetry outside the model domain in 30-35 m water depth shows the presence of large scale bedforms, which, if they are not relict features, suggest sand transport occurs in deep water in the southern Gulf of St. Lawrence. In deep water, waves with peak period of 9.5 s (such as are indicated at the hindcast node at the height of the storm; Fig. 19) can be considered to have a wavelength of approximately 140 m ($L_o=gT_o^2/2\pi$) giving a wave base of 70 m ($L_o/2$). It is therefore quite conceivable that sand transport can occur throughout the model domain during storms.

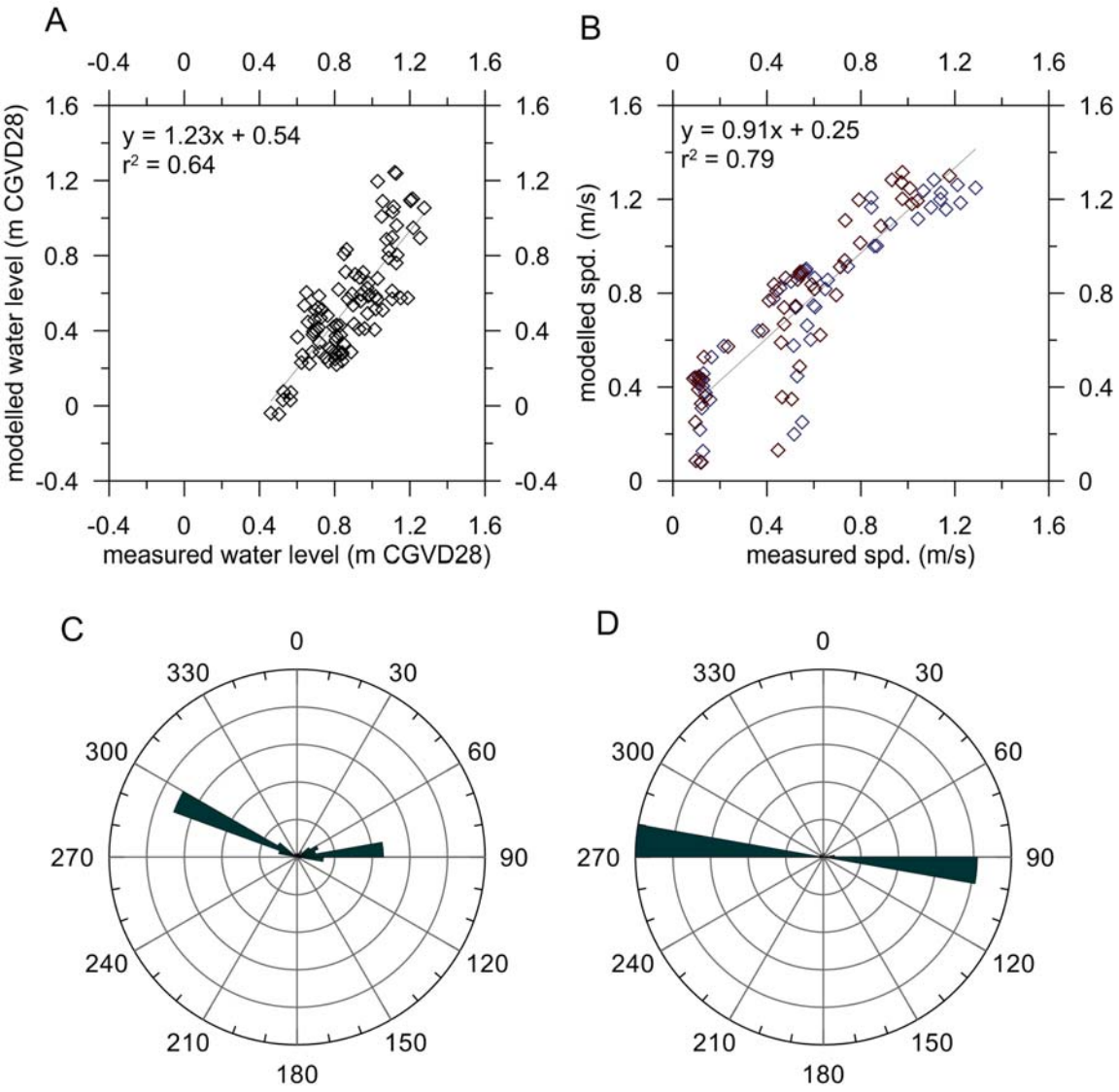

Figure 22. Correlation between measured and modelled water levels (A) current speeds (B) and the directional histograms of measured (C) and modelled (D) current directions. Modelled and measured water levels are correlated with r^2 value of 0.64 and RMS error of 0.38 m, and current speeds are correlated with r^2 value of 0.79 and RMS error of 0.25 m/s. The circular correlation coefficient between measured and modelled current directions is 0.27 with RMS error of 45.99 degrees. Rings are in increments of 10 samples.

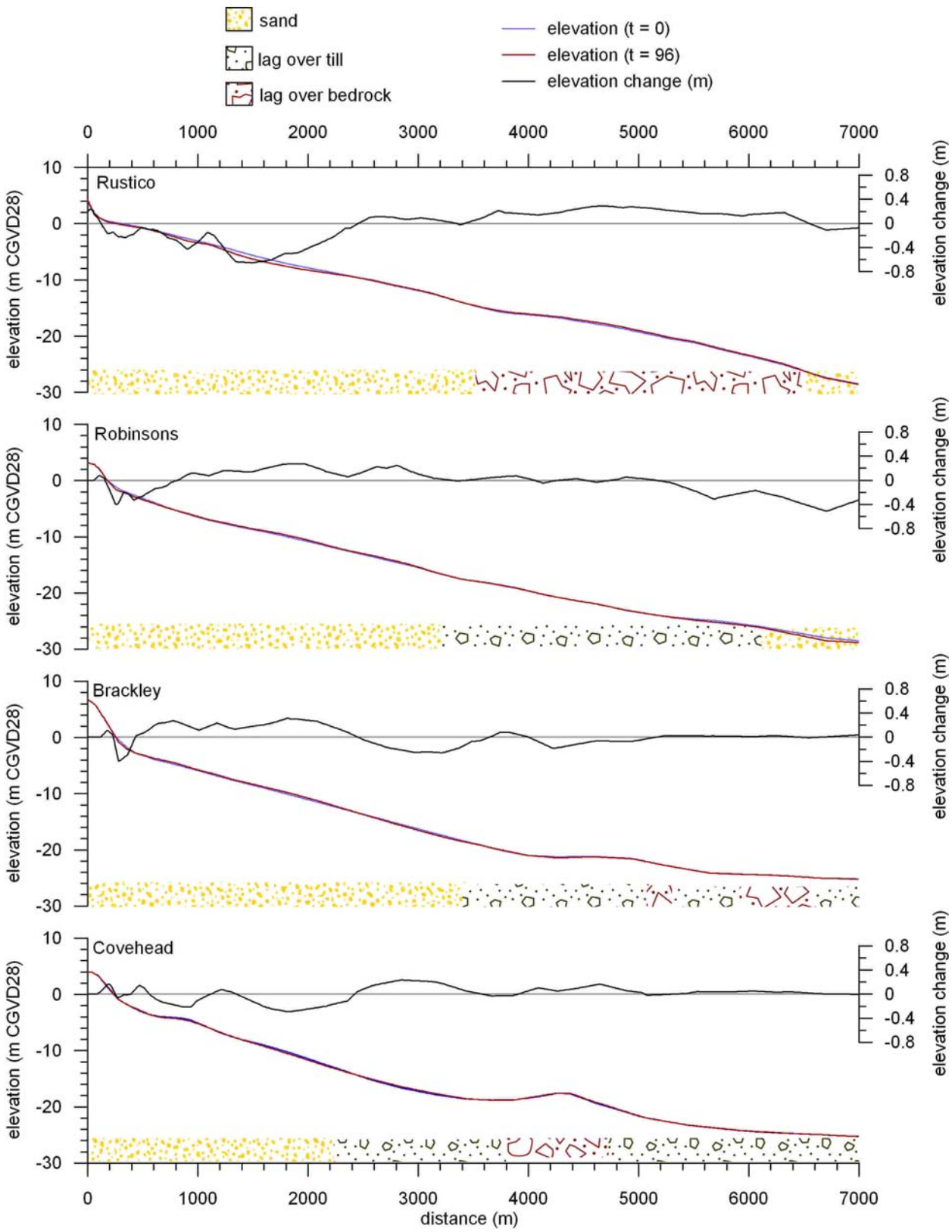

Figure 23. Results from the final configuration of the ST module of profiles and elevation change. Also shown are the sediment classes along each profile.

Overall, the spatial distribution of sediment transport simulated in Run28 (Fig. 18) appears reasonable. Winds during the Dec. 2 1999 storm reached their maximum from the northeast suggesting nearshore sand transport should be to the west. The model predicts this in general, and Run28 improves on previous configurations (Figs. 14 and 15) which developed some areas of abrupt changes in transport direction corresponding to changes in seabed sediment class. Excluding streaming (mass transport by wave-driven currents in the wave boundary layer), and slight modification to the sediment class definitions appears to eliminate the phenomenon.

Another result that appears to have been improved in Run28, is where a clockwise transport node developed in some simulations at the storm peak off Stanhope Cape which forms the divide between Brackley Bight and Stanhope Bight. In Figure 15, sediment transport in the offshore is directed onshore then turns to east, while the flow in the nearshore is onshore and then along shore to the west. The water (and suspended sediment) at C between these two streams with opposite directions may be entrained to result in the clockwise eddy of sediment transport direction at C. In Run28 (Fig. 18), this complexity in sediment transport is reduced and a more likely condition of transport to the east and west at the Stanhope Cape headland is simulated. This fits with conceptual understanding of subtle headlands along the North Shore of PEI forming drift divides and divisions between morphological cells (Forbes et al., 2004).

A final result requiring future consideration is the development of the alongshore cell-like structure in erosion and deposition. This suggests the model may be simulating rip current effects or trapped waves, and may be capable of producing nearshore bars and simulating shoreline changes if run for longer duration.

Conclusions

A configuration of Mike21 Flexible Mesh can be developed for Brackley Bight that, when compared to instrument data, successfully simulates waves, currents and sediment transport during a mild northeasterly storm affecting the southern Gulf of St. Lawrence. The domain measures approximately 13 km alongshore and 7 km in the cross-shore direction. Elevations in the domain are obtained from a combination of LiDAR, and water depths from multibeam bathymetry and CASI. Seabed sediments are characterised using multibeam backscatter, and information from camera drops and ROV tows, grab sampling and coring. The model involves simultaneous runs of the Spectral Wave, Hydrodynamic and Sand Transport modules at an hourly master timestep, and simulates 4 days from November 30 to December 3 1999, with a run time of approximately one hour.

Significant wave height, peak period and direction are well simulated in the Spectral Wave module. This module is somewhat sensitive to variations in the wind forcing formulation and wave breaking parameters, but more sensitive to adjustments in the Nikuradse coefficient describing bottom friction. It was found that the optimal value corresponds to the median grain size, d_{50} in the three mapped sediment classes.

Current speeds are reasonably well simulated in the Hydrodynamic module, though some anomalies develop at the beginning and end of the simulation. Current directions show a strong alongshore orientation in contrast to measured directions which include a significant cross-shore component. The accentuated alongshore component in current direction is considered a result of comparing direction measurements from 0.6 m above the seabed, with depth-averaged directions from the model. Another contributing factor may be the simplified bathymetry used in the model. Incorporating more complex bathymetry from a previous model run may alleviate this issue. Water levels are well simulated during the storm peak but are underestimated at the beginning and end of the storm. The poorer performance of the Hydrodynamic module relative to the Spectral Wave module may be a result of the use of predicted tides as boundary conditions, and the relatively small domain in which the larger circulation in the southern Gulf of St. Lawrence cannot be incorporated. The Hydrodynamic module is highly sensitive to variations

in the wind friction coefficient and to a lesser extent the Manning number, with the wind friction coefficient affecting both current speed and water level and the Manning number affecting current speed. It was found that a Manning number calculated from the Nikuradse coefficient equal to d_{50} is optimal. With this optimal Manning number, an optimal wind friction coefficient of 0.004 was adopted.

In this treatment, consideration of the results of the Sand Transport module relies upon conceptual understanding and anecdotal evidence rather than direct measurement. It is believed that the results are reasonable, with prominent alongshore drift as expected, a drift divide produced at Cape Stanhope which fits conceptual understanding, and sediment transport into the inlets, also fitting conceptual understanding. The Sand Transport module is sensitive to the required sediment transport tables produced from the stand-alone STPQ3D routine; it was found that a simple sediment transport table is as effective as a more complex one, and excluding mass transport by wave-driven currents reduces, but does not eliminate, abrupt changes in transport direction. The best results from the Sand Transport module were obtained when the coarse sediment classes were modified to include a sand fraction, allowing bypass and transport in these classes. The Sand Transport module is also slightly sensitive to the theshold thickness of the mobile sediment layer, for which a value of 0.5 m was adopted, and very sensitive to the maximum allowable change per day in bed level, for which it is thought a value of 0.25 m/day is reasonable. This value is supported to a certain degree by underwater video observations of vertical erosion.

This research is part of a larger project directed towards understanding the impacts of changing climate on sediment transport on the North Shore of Prince Edward Island. Next steps include using the configuration of Mike21 to simulate other storms, and extend the run duration to include entire seasons. An approach to include spatially and temporally varying sea ice and its effects on wave formation and propagation will also be investigated.

Acknowledgements

This research was conducted under the ESS Program on Enhancing Resilience to Changing Climate and as part of the authors doctoral research at the University of Guelph. Funding provided by the University of Guelph in the form of two graduate scholarships, and support from the ESS Professional Enhancement Program are gratefully acknowledged. Azhural Hoque was very helpful in the initial stages of developing the model, and discussions with Donald Forbes on the coastal morphology and processes of the study area are greatly appreciated. Of course none of this work would be possible without the efforts of Donald Forbes, Steve Solomon, and the crews of CCGS Hudson, CCGS Matthew, CCGS Creed, CSL Plover, PWGS Launches Miramichi Surveyor and Scotia Surveyor, and MV Gulf Explorer. Tim Webster and others with the Centre of Geographic Sciences were instrumental in the LiDAR data collection, processing and validation, and Hyperspectral Data International collected and processed the CASI data with bathymetric post-processing by Yann Morel. All are gratefully acknowledged. Internal review by Michael Li and comments by Robin Davidson-Arnott and Jeff Ollerhead were highly beneficial in improving this manuscript; their work is greatly appreciated.

References

DHI, 2007. Mike 21 and Mike 3 Flow Model FM Training Guide. Danish Hydraulics Institute, Horsholm.

Doering, J.C. and Bowen, A.J., 1995. Parameterization of orbital velocity assymetries of shoaling and breaking waves using bispectral analysis. Coastal Engineering, 26: 15-33.

Dupont, F., Hannah, C.G., Greenberg, D.A., Cherniawsky, J.Y. and Naimie, C.E., 2002. Modelling system for tides for the northwest Atlantic coastal ocean. Canadian Technical Report of Hydrography and Ocean Sciences, 221: vii + 72.

Forbes, D.L. and Manson, G.K., 2002. Coastal geology and shorezone processes. In: D.L. Forbes and R.W. Shaw (Editors), Coastal Impacts of Climate Change and Sea-Level Rise on Prince Edward Island, Geological Survey of Canada Open File 4261, pp. 85.

Forbes, D.L., Parkes, G.S., Manson, G.K. and Ketch, L.A., 2004. Storms and shoreline retreat in the southern Gulf of St. Lawrence. Marine Geology, 210: 169-204.

Hasselmann, D.E., Dunckel, M. and Ewing, J.A., 1980. Directional wave spectra observed during JONSWAP (1973). Journal of Physical Oceanography, 10: 1264-1280.

Holthuijsen, L.H., Booij, N. and Herbers, T.H.C., 1989. A prediction model for stationary, short-crested waves in shallow water with ambient current. Coastal Engineering, 13: 23-54.

Johnson, H.K., 1998. On modeling wind-waves in shallow and fetch limited areas using the method of Holthuijsen, Booij and Herbers. Journal of Coastal Research, 14: 917-932.

Kahma, K.K. and Calkoen, C.J., 1994. Growth curve observations. In: G.J. Komen et al. (Editors), Dynamics and Modelling of Ocean Waves. Cambridge University Press, Cambridge, pp. 174-182.

Keen, T.R., Beavers, R.L., Howd, P.A. and Hathaway, K., 2003. Shoreface sedimentation during a northeaster at Duck, North Carolina, U.S.A. Journal of Coastal Research, 19: 24-40.

Li, M.Z. and Heffler, D.E., 2002. Environmental marine geoscience 3. Continental shelf sediment transport studies in Canada: Theories and recent technology advances. Geoscience Canada, 29: 35-48.

Morel, Y.G., 1996. A coral reef as seen by SPOT, Proceedings, 8th Australasian Remote Sensing Conference, Canberra, pp. 1-14.

Parkes, G., Forbes, D.L. and Ketch, L., 2002. Sea-level rise. In: D.L. Forbes and R.W. Shaw (Editors), Coastal Impacts of Climate Change and Sea-Level Rise on Prince Edward Island, Geological Survey of Canada Open File 4261, pp. 85.

Ruessink, B.G., Walstra, D.J.R. and Southgate, H.N., 2003. Calibration and verification of a parametric wave model on barred beaches. Coastal Engineering, 48: 139-149.

Soulsby, R., 1997. Dynamics of Marine Sands. Thomas Telford, London, 249 pp.

Swail, V.R. et al., 2006. The MSC50 wind and wave reanalysis, 9th International Workshop On Wave Hindcasting and Forecasting, Victoria, B.C. Canada, pp. 29.

USACE, 1973. Shore Protection Manual. Coastal Engineering Research Centre, Vicksburg.

USACE, 1984. Shore Protection Manual. Coastal Engineering Research Centre, Vicksburg.

Webster, T.L., Forbes, D.L., Dickie, S., Covill, R.A. and Parkes, G.S., 2002. Airborne imaging, digital elevation models and flood maps. In: D.L. Forbes and R.W. Shaw (Editors), Coastal impacts of climate change and sea-level rise on Prince Edward Island, Geological Survey of Canada Open File 4261, pp. 31.

Webster, T.L., Forbes, D.L., MacKinnon, E. and Roberts, D., 2006. Flood-risk mapping for storm-surge events and sea-level rise using LiDAR for southeast New Brunswick. Canadian Journal of Remote Sensing, 32: 194-211.